Department of Physical Sciences

Indian Institute of Science

Education and Research, Kolkata

Master Thesis in Physics

submitted by

Arikta Saha

Department of Physical Sciences

IISER Kolkata

May 2024

Controlling resonant absorption in helium using intense XUV FEL pulses in combination with HHG transient-absorption spectroscopy

Master Thesis

which is being carried out by Arikta Saha

under the supervision of

Dr. Christian Ott

at Max-Planck-Institut für Kernphysik in Heidelberg

Acknowledgement

I would like to thank everyone in the group for the nice, funny, instructive and always entertaining time during this dissertation and for supporting me through this journey. The successful completion of a master's thesis relies on the collaboration of a competent team, enough support, and a conducive working environment. It is not only dependent on the efforts of one person. I express my heartfelt gratitude to the Department of Physical Sciences at IISER Kolkata for granting me the opportunity to do my MS thesis study at MPIK Heidelberg. This chance was really helpful to my academic path. I would like to give my special thanks to...

Dr. Christian Ott who gave me the opportunity to do this work. Your expertise and insightful feedback were instrumental in shaping my research and pushing me to achieve my best. I was able to gain a lot from your advice.

Prof. Dr. Thomas Pfeiffer who inspired me about physics and taught me how to think beyond. Thank you for the initial review of this work. Thank you for teaching something from every conversation with you.

Harijyoti Mandal who accompanied me in managing things during the beamtimes at FLASH. Thank you for all the fun activities and chat in Bengali we had together.

Dr. Ulrike Frühling who assisted us in the beamtime and helped us in having a successful beamtime.

Dr. Stefan Düsterer who helped us in tuning the FEL from the synchrotron source tunnel and allowed the smooth functioning of the beamtime.

Dr. Christina Papadopoulou & Dr. Elisa Appi who built the high harmonic generation setup and were managing it during the beamtime working with us day and night. Thank you for your dedication in keeping the lab records detailed.

Christian Kaiser who assisted in the construction of the black box for the optical setup at FLASH beamline.

Dr. Rui Jin who helped me understand the intricacies of the theories and helped me get a better overall understanding. Thank you for all the funny conversations we had together.

Dr. Yu He who answered my many short questions. Thank you for encouraging me and taking me to the gym and telling me to take care of my health during this last year.

Dr. Gergana Borisova who taught me so many crucial things. Thank you for all the tips on thesis, python and graphics.

Dr. Carlo Kleine for the many funny conversations we were able to have together and who always had an open ear for me at the beginning of my work.

Muwaffaq Ali Mourtada for all the interesting and funny conversations during the coffee and all the fun we had during the tiring beamtimes.

Abstract

Studying the dipole response of the excited quantum system could provide insights into the extreme ultraviolet (XUV) light-matter interaction. Transient absorption spectroscopy uses the dipole response field's interaction with incoming light to leave a signature on the transmitted light. This thesis uses high-harmonic generation (HHG) and free electron lasers (FEL) as XUV light sources, with helium serving as the subject of interest. We study the absorption lineshape of singly excited state resonances of helium in a delay-resolved manner using a delay stage, which we can detect in single-shot mode on our XUV spectrometer. The study aimed to understand the perturbations in HHG-induced atomic dipole responses when there is interaction with intense FEL pulses. The XUV HHG pulses first excite the absorption lineshape, and intense XUV FEL pulses further modify it. It leads to a change in the absorption feature. The linewidth broadening indicates the dynamics of the interaction of the XUV pulses with the excited states in helium. The perturbed dipole response function can be used to determine how the XUV-driven excited state dynamics evolve in real-time. The femtosecond-level time-delay-resolved absorption spectra have been recorded at different helium target gas pressures, FEL intensities, and FEL photon energies. The experiment was conducted at beamline FL26 in the free electron laser (FEL) FLASH 2 facility in DESY Hamburg, which generated tunable intense SASE FEL pulses of 20 μJ, 50 fs of pulse length, and a single bunch pulse train with a repetition rate of 10 Hz. In this work, an attempt has been made to adapt the dipole control model to the FEL interaction and the resulting plasma environment.

List of Figures

List of Tables

Contents

1 Introduction

The atoms that make up a star are kept in an exotic environment of plasma. What kind of behaviour the atoms show in such stellar environment? How do they interact with the strong field inside the star? The answer to these questions are important for understanding the stellar entities and verify the parameters for the stellar evolution models. The dynamics of these interaction is also of the same importance. The dynamics of such interaction occur on an ultrafast timescale such as picosecond to attosecond and thus needs methods which are even more precise. There is only one such method to study such ultrafast dynamics that using ultrashort laser pulses.

In stellar entities like the sun, hydrogen is the most abundant element but in some cases there can be plasma without any hydrogen. So helium lines can be used which has an advantage of being a non-reactive gas[10]. Helium is also the smallest bound multielectron system with two electrons bound to the core[26]. Thus, in this thesis, helium is selected as the preferred quantum system.

In stellar environment like the solar corona, intense extreme ultraviolet(XUV) light is produced by the plasma. There is only one source of radiation which can provide such laser i.e., synchrotron. The synchrotron at DESY is used to produce intense XUV ultrashort pulses with the undulators at Free Electron LAser in Hamburg(FLASH). The high intensity of FELs enables the reliable ionisation of a significant number of helium atoms in the gas cell.

The interaction dynamics of plasma can accessed through studying the rate of decay of the singly excited resonance states of helium. The resonance states needs to excite and recorded in a spectrum as absorption. For such excitations, a broad range of XUV photon energies in needed and the spectrum must be stable enough to record the absorption signal but weak enough such that the excited atoms are low in population and in general isolated from other excited atoms. This purpose has been served by high harmonic genera-

tion(HHG) pulses which is generated from an infrared(IR) pulse at the HHG hut at Beamline FL26.

The dynamics were observed for different parameters such as pressure i.e., the backing pressure of the target gas cell and intensity of FEL attenuated through inserting Aluminium filters. These experiments were conducted to determine the optimal settings for the generation of plasma. The photon energy of the FEL has also been tuned below and above the first ionization threshold of helium i.e., 24.587 eV in order to confirm the occurrence of strong field ionisation and plasma generation.

This experiment employs a control-probe approach where the alterations in the material i.e., absorption are made by illuminating the gas with ultrashort laser pulses the information about which is encoded in the laser spectrum before and after hitting the target. This absorption lineshape can be used to reconstruct the dynamics in the material due to the light matter interaction. The spectrum is recorded near the temporal overlap of HHG and FEL pulses for different time delay range. This will help in evaluating the absorption changing with relative delay between the two pulses.

The atomic dipole response $d(t)$ of the system can be reconstructed from the single time delay absorption signal which can be used to study the real-time dynamic of the system[24]. In previous table-top HHG experiments, such the dipole responses were excited by the HHG and then after certain time delay perturbed by NIR pulses which resulted in the modification of the absorption lineshape[24]. But in this experiment which is first of its kind, the NIR pulse is replaced by a XUV SASE FEL pulse to perturb the decay of the coherent dipole response excited by HHG-XUV resonant interaction and control or modify the coherence in a state-specific manner by non-resonant absorption of XUV FEL. The XUV transmitted spectrum is recorded by the high-resolution XUV spectrometer

In this experiment, when the Free Electron FEL is the first pulse, it ionises the helium atoms in the gas cell, resulting in the generation of plasma. After

a time delay τ, the HHG pulse probes the system by exciting resonant transitions. On the other hand, when the HHG pulse is the first pulse, it excites the resonant transitions, and after a time delay τ, the FEL pulses ionise the helium atoms and induce the plasma effect. This will provide information regarding the impact of plasma on resonances.

The thesis is arranged in the following manner: In the following chapter 2, the fundamental scientific concepts required for the experiment have been introduced. In chapter 3, the experimental setup has been described in details along with the setup calibrations. In chapter 4, the procedure to analyse the experimental data has been described. In chapter 5, a model has been adapted from the dipole control model[4].

2 Fundamental Scientific Theory

This chapter will emphasise on the fundamental concepts of ultrafast ionization dynamics and nonlinear interaction of intense and ultrashort XUV laser pulses with matter and their mathematical descriptions which are important to understand and interpret the physical processes occuring in the experiment presented in this thesis. In this thesis, ionization of helium and its effect on state-specific resonant excitation is studied in the helium atom.

2.1 Quantum Dynamics

An atom, as a quantum system, may be characterised by quantum states that are composed of a superposition of bound(discrete) states $|\psi_i\rangle$ and continuous states $|\phi_E\rangle$.

$$|\psi\rangle = \sum_i c_i |\psi_i\rangle + \int dE c(E) |\phi_E\rangle \tag{2.1}$$

Only the bound states are considered for the purpose of this thesis. The interaction of a quantum system with external fields leads to a dynamic transition between different states of the system. The state and dynamics of a quantum mechanical system are characterized by the wavefunction Ψ and its time-evolution. In non-relativistic quantum mechanics, the dynamics of the quantum system are governed by the time-dependent Schröndinger equation:

$$i\frac{\partial}{\partial t} |\psi(t)\rangle = \hat{H} |\psi(t)\rangle \tag{2.2}$$

The Hamiltonian operator $\hat{H}$ can be written as:

$$\hat{H} = \hat{H}_0 + \hat{H}_{int} \tag{2.3}$$

where $\hat{H}_0$ is the Hamiltonian of the unperturbed system and $\hat{H}_{int}$ is the change in energy of the system due to the external interaction.

The equation 2.2 can be expressed in two different forms: the Schrödinger-picture, where the time dependence is carried by the state vector represented by the wave function, and the Heisenberg picture, where the operators are time-dependent and the state vector remains independent of time. Alternatively, it may be described using the interaction picture, which combines elements from both the Schrödinger and Heisenberg pictures. In this picture, the evolution caused by H_0 is transferred to the operators.

$$|\psi(t)\rangle_I = e^{i\hat{H}_0 t} |\psi(t)\rangle_S \qquad\qquad |\psi(0)\rangle_I = |\psi(0)\rangle_S \tag{2.4}$$

The Hamiltonian $\hat{H}$ can be represented by a n×n Hermitian matrix and the wavefunction $|\psi(t)\rangle$ in terms of an n-dimensional state vector.

$$\hat{H} = \begin{pmatrix} E_1 & W_{12} & \cdots & W_{1n} \\ W_{21} & E_2 & \cdots & W_{2n} \\ \vdots & \vdots & \ddots & \vdots \\ W_{n1} & W_{n2} & \cdots & E_n \end{pmatrix} \qquad\qquad |\psi(t)\rangle = \begin{pmatrix} c_1(t) \\ c_2(t) \\ \vdots \\ c_n(t) \end{pmatrix} \tag{2.5}$$

where Hamiltonian $\hat{H}$ describes the energy of the quantum system, E_j are the energies of the n discrete states, c_j are the complex coefficients of the different states and W_{ij} are the coupling matrix elements between states i and j.

The perturbation in the case of a system interacting with a linearly polarized light in dipole approximation can be written as

$$\hat{H}_{int} = \hat{d}.E(t) \tag{2.6}$$

where $\hat{d} = -e \cdot \hat{x}$ the dipole operator

In the case of weak field interaction, the quantum system could be understood with Time-Dependent Perturbation theory. However, if the field strength is high, the dynamics occur in a regime of strong coupling where the perturbation

theory does not apply.

The coupling matrix elements are time-dependent and in the case of pure dipole interaction can be written as

$$W_{ij} = \langle \psi_i | \, \hat{d}E(t) \, | \psi_j \rangle = d_{ij}E(t) \tag{2.7}$$

2.2 Transient Absorption Spectroscopy

The process of shining light on materials and analysing the resulting spectrum intensities is a fundamental method used in several scientific disciplines. The interaction kinetics and internal structural information may be inferred by analysing the absorption change resulting from the sample interaction. The observed spectra are correlated with the parameters of the target by using the relationship between gas absorption and the microscopic dipole moment in the atoms.

2.2.1 The dipole response and the absorption

In the presence of a light field, the system is coherently excited which scatters all non-interacting atoms in a dilute gas target. Thus it can be considered as a single-atom quantum system the atom is excited and a time-dependent dipole moment is initiated. In terms of quantum mechanics, it can be considered as a superposition of the excited state and the ground state which gives us an exponentially decaying and oscillating expectation value of the dipole operator. Electrons in a classical context are driven by the oscillating electric field $E(t)$ of the light wave, forcing them to undergo oscillatory motion. The material's macroscopic polarization P can be attributed to the averaged microscopic dipole moment $\langle d \rangle$ of the material's constituent, which is given by:

$$P = \rho_N \langle d \rangle \tag{2.8}$$

where ρ_N denotes the number density of the material.

The microscopic dipole moment interacts with the electromagnetic waves in the form of macroscopic polarization P, which is given by the simplified wave equation:

$$\left[\frac{\partial^2}{\partial z^2} - \frac{1}{c^2}\frac{\partial^2}{\partial t^2}\right] E(t,z) = \mu_0 \frac{\partial^2}{\partial t^2} P(t,z) \tag{2.9}$$

where μ_0 is the vacuum permittivity and z is the direction of propagation of the electromagnetic waves.

In eqn 2.9, the polarization results in the generation of the electric field. The field generated by the polarization interferes with the incident laser field resulting in a modified field. Destructive interference leads to a reduction of the field, which is known as absorption. Constructive interference occurs when the field amplitude is increased, resulting in a net gain. The experiments conducted in this thesis only focus on dilute gas targets, thus the propagation effects can be neglected. The linear polarization can be written in the frequency domain by performing a Fourier transform:

$$\tilde{P}(\omega, z) = \varepsilon_0 \chi(\omega) \tilde{E}(\omega, z) \tag{2.10}$$

2.2.2 Optical Density(OD)

The atomic dipole response and its dynamics can be tracked by observing the intensity of the transmitted light. It is desirable if the intensity is independent of the incident laser field and for that, it is suitable to calculate the optical density which is given by:

$$OD = -\log 10 \left(\frac{I(\omega)}{I_0(\omega)}\right) \tag{2.11}$$

where $I(\omega)$ and $I_0(\omega)$ are the intensity of the transmitted radiation and incident radiation respectively.

The optical density can be linked with dipole response with the equation

$$\begin{aligned} OD &= -\log_{10}\left(\frac{I(\omega)}{I_0(\omega)}\right) = \frac{\rho L}{ln(10)}\frac{\omega}{\varepsilon_0 c} Im\left(\frac{d(\omega)}{E_{in}(\omega)}\right) \\ &= \frac{(\rho L)_{a.u.}}{ln(10)} 4\pi\alpha\omega Im\left(\frac{d(\omega)}{E_{in}(\omega)}\right) \end{aligned} \tag{2.12}$$

where the expression in the second line is in atomic units.

From a time-domain perspective, the whole dipole response is recorded in a time-integrated manner hence temporal sampling of the dipole response is not possible. The temporal resolution in transient absorption measurement depends on the time delay, while the 'real' time evolution of the dipole response is encoded in the spectrum.

Differential Optical Density(ΔOD)

The change in absorption induced by the perturbative field which in this case is an intense FEL is a more qualitative measure of the microscopic ultrafast electron dynamics. In this method, the transmitted spectra are recorded with and without FEL ($I_{ON}(\omega)$ and $I_{OFF}(\omega)$. The change in optical density (ΔOD) is given by:

$$\begin{aligned} \Delta OD &= OD_{ON} - OD_{OFF} \\ &= -\log_{10}\left(\frac{I_{ON}(\omega)}{I_0(\omega)}\right) + \log_{10}\left(\frac{I_{OFF}(\omega)}{I_0(\omega)}\right) \\ &= -\log_{10}\left(\frac{I_{ON}(\omega)}{I_0(\omega)}\frac{I_0(\omega)}{I_{OFF}(\omega)}\right) \\ &= -\log_{10}\left(\frac{I_{ON}(\omega)}{I_{OFF}(\omega)}\right) \end{aligned} \tag{2.13}$$

In the absence of FEL tuning over the ionisation threshold, the absence of ions results in the absence of any absorption, save for the neutral target. When the primary emphasis is on the absorption of ions, the optical density (OD) encompasses all the relevant information and even eliminates some background absorption from the neutral particles.

2.3 The Dipole Control Model

The temporal dipole response d(t) of an excited state $|e\rangle$ after excitation from the ground state $|g\rangle$ by a Dirac δ like function pulse at t=0, e.g. by an attosecond XUV-HHG pulse is taken as the starting point. The dipole response has an exponential decay rate Γ, and oscillates at the resonance frequency ω_r. The 1^{st} order perturbation theory has been used to calculate the dipole response:

$$c_e(t) = \frac{1}{i\hbar} d_{eg} E_{ex} \tag{2.14}$$

The full wavefunction $|\Psi(t)\rangle$ of our model system evaluates to:

$$|\Psi(t)\rangle = |g\rangle + \frac{1}{i\hbar} d_{eg} E_{ex} e^{i\omega_{eg}t - \Gamma/2t} |e\rangle \tag{2.15}$$

The temporal dipole moment can be derived as the expectation value of the dipole operator and considering the relation $d_{eg} = d_{eg}^*$

$$d(t) = \langle\Psi| \hat{d} |\Psi\rangle = \frac{i}{\hbar} |d_{eg}|^2 e^{i\omega_{eg}t - \Gamma/2t} \tag{2.16}$$

This gives an unperturbed decaying dipole response as given in Fig 2.1 which reduces to

$$d_j(t) = i d_{ge}^2 e^{i\omega_{r_j} t - \frac{\Gamma_j}{2} t} \tag{2.17}$$

Here d_{ge} is the dipole matrix element for transition $|g\rangle \rightarrow |e\rangle$.

The spectral response of the dipole moment or the absorption crosssection of the system is proportional to the imaginary part of the Fourier transform of eqn 2.17. It is given as:

$$\sigma(\omega) = \omega \mathbb{Im}\left(\frac{\tilde{d}(\omega)}{\tilde{E}(\omega)}\right) = \omega \mathbb{Im}\left(\frac{\mathcal{F}[d(t)]}{\mathcal{F}[E(t)]}\right) = \frac{\omega}{E_0} \mathbb{Im}\left(\int_0^\infty d(t) e^{i\omega t}\right) \tag{2.18}$$

where $E(t)$ is the excitation pulse (HHG) which can be approximated as a Dirac δ pulse $E(t) = E_0 \cdot \delta$. The spectrum of the δ-like pulse is uniformly

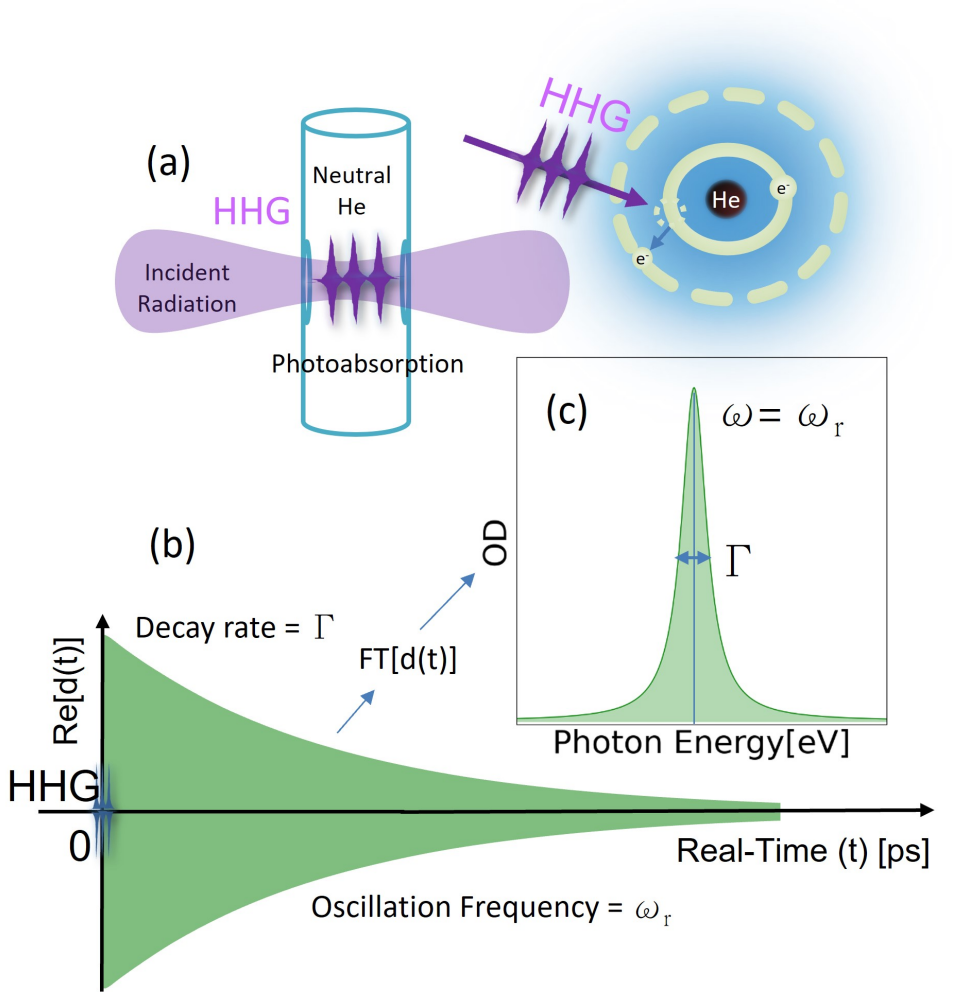

Figure 2.1: (a) Neutral helium in the target gas cell is excited with XUV HHG pulse to singly excited states. (b) The excitation is followed by a free oscillating dipole decay with decay rate of Γ and an oscillating frequency of ω_r. (c)The spectral response is calculated using the Fourier transform of the dipole response

distributed, and hence, within a certain range of frequencies, it may be approximated by $\mathcal{F}[E(t)] = E_0$

2.4 The helium atom

The helium atom consists of a doubly charged nucleus and 2 electrons which makes it the simplest multi-electronic system. The wavefunction of the helium

atom can be described as

$$\Psi(q_1, q_2) = \psi(r_1, r_2)\chi(s_1, s_2) \tag{2.19}$$

where ψ denotes the spatial degree of freedom and χ denotes the spin wave function of the two-electron system.

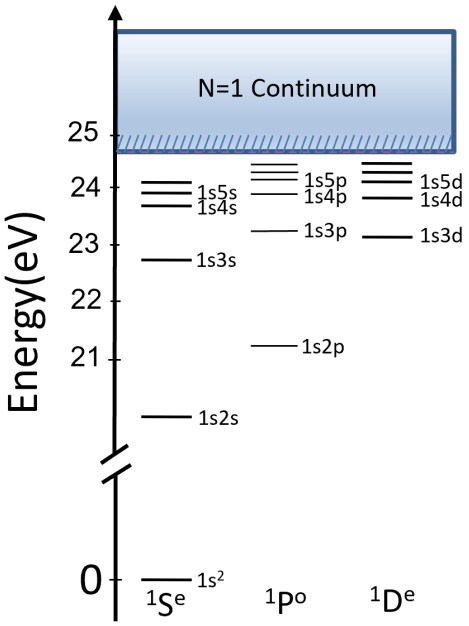

Figure 2.2: Energy scheme of the helium atom: The data of resonance energy are taken from [9]

In a multi-electron system like helium, the states can be represented by the notation $nl_1ml_2\ ^{2S+1}L^{\lambda}$, where n,m are the principal quantum numbers, l_1, l_2 are the respective angular momentum, S denotes the quantum number of the total spin, L indicates the quantum number of total angular momentum and λ denotes the parity of the states which can be odd(o) or even(e). All the resonance states that are spectroscopically inspected in this work are singlet (S=0) states with an asymmetric spin wave function $\chi(s_1, s_2)$. The spatial wavefunction is symmetric following Pauli's principle for fermions. In the dipole approximation of laser interaction, only transitions between states with

differing parity are allowed. This implies that the ground state of helium i.e., $1s^2$ is a $^1S^e$ state that can be excited to $^1P^0$ state via a single-photon excitation.

The extensive photon energy range of the high harmonic generation allows the investigation of multiple configurations of excited electronic states in helium. The energy levels of helium that can be excited via a single XUV photon absorption span from 21.22 eV for 1s2p from the $1s^2$ ground state to 78.98 eV which is the threshold for complete ionization. The first ionization threshold, i.e., the energy required for one electron to overcome the coulomb force is 24.59 eV which is the highest in all atoms. The literature values of the energy levels and the decay rates of dipole-allowed singly excited states have been summarized in Table 2.1.

Table 2.1: Energies and decay rates of 1snp singly excited states of helium were taken from [9]

Configuration	Energy (eV)	Decay Rate Γ (meV)
$1s^2$	0	
1s2p	21.218	0.0074
1s3p	23.087	0.0023
1s4p	23.742	0.001
1s5p	24.046	0.0005
1s6p	24.211	0.0003

2.5 Broadening of Absorption Lines

When radiation is absorbed or emitted during an atomic transition, it does not produce a strictly monochromatic spectral line. Instead, it creates a range of frequencies centred around the frequency ν_0 as given in Fig 2.3. The linewidth of the spectral profile is the full width at half-maximum. The width of the line profile is influenced not only by the spectral resolution of the measuring instrument, but also by fundamental physical characteristics, such as the life-

times of the atomic states involved in the transition, the velocity distribution of the moving atoms, and the pressure of the gaseous sample. The spectral interval inside the full half-width is called the line kernel, the ranges outside the line wings. There are several contributing factors to the lineshape broadening

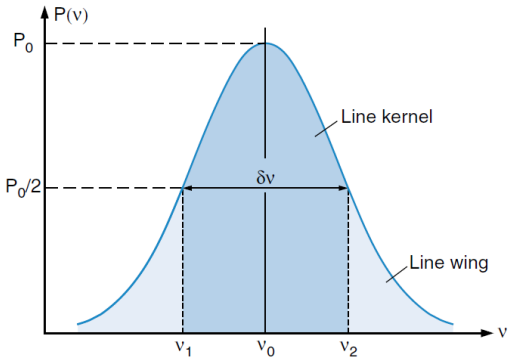

Figure 2.3: Spectral Line Profile: Figure taken from [7]

which have been discussed here.

2.5.1 Natural Broadening

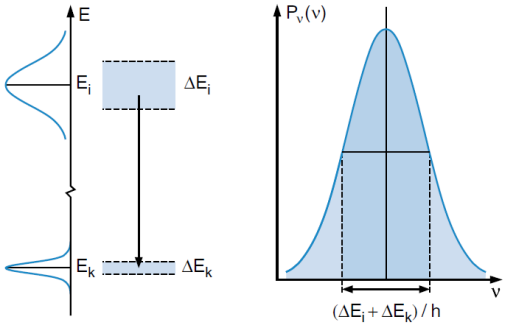

Figure 2.4: Natural linewidth caused by the energy uncertainties ΔE_i, ΔE_k of the atomic levels involved in the transition $h\nu_{ik} = E_i - E_k$: Figure taken from [7]

The energy levels of the atoms possess an energy uncertainty $\delta E = h/\tau$, related to their finite lifetime τ. The spectral line's frequency width, which corresponds to the transition between levels E_i and E_k, is

$$\delta\nu_{ik} = \delta E_i + \delta E_k/h \tag{2.20}$$

An excited atom can deliver its excitation energy in the form of spontaneous emission. The excited electron will be described by the classical model of a damped harmonic oscillator with mass m, spring constant D and eigenfrequency $\omega_0 = \sqrt{D/m}$ (Hertzian dipole). The time-dependent amplitude of its oscillation can be obtained from the equation of motion

$$\ddot{x} + \gamma\dot{x} + \omega_0 x^2 = 0 \tag{2.21}$$

where γ is the damping constant. The solution for eqn 2.21 with the approximation of $\gamma << \omega_0$ is:

$$x(t) \approx x_0 \exp^{-(\gamma/2)t} \cos(\omega_0 t) \tag{2.22}$$

The Fourier transform of $x(t)$ gives the frequency line profile which is given by:

$$P_\omega(\omega) = P_0 \frac{\gamma/2\pi}{(\omega - \omega_0)^2 + (\gamma/2)^2} \tag{2.23}$$

is called the Lorentzian Profile. The full width at half maximum is called the natural linewidth i.e.,γ because it is caused by the spontaneous emission of the atom, without any external influences.

2.5.2 Doppler Broadening

The excited atoms in a gas will be moving at different velocities. The Doppler effect causes a change in the colour of each emitted photon, either towards red or blue, depending on the relative velocity of the atom and the observer. As the temperature of the gas increases, the range of velocities in the gas also increases. The spectral line is wider as the temperature of the gas is greater because it is a composite of all emitted radiation.

The spectral profile of Doppler broadened lineshape is given by:

$$A(\omega) = A(\omega_0) \exp^{-(\frac{\omega-\omega_0}{\omega_0})^2 \frac{m}{2k_B T}} \tag{2.24}$$

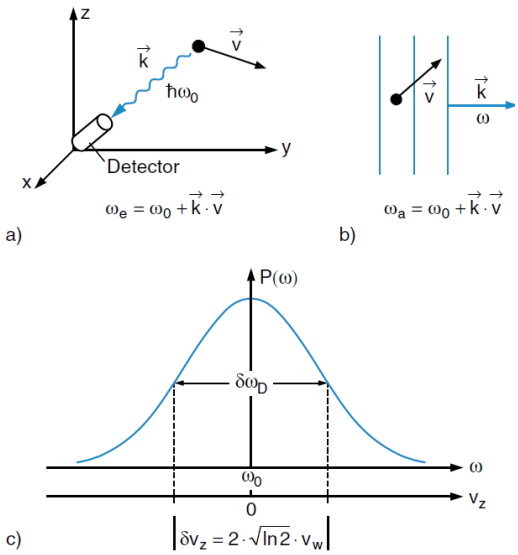

Figure 2.5: Doppler Broadening:(a)Emission with doppler-shift (b)Photons absorbed (c)Doppler broadened gaussian profile: Figure taken from [7]

The full width half maxima of doppler broadened lineshape is given by:

$$\delta\omega_D = \frac{\omega_0}{c}\sqrt{\frac{8k_BTln2}{m}} \tag{2.25}$$

3 Design of the experimental apparatus

At the very heart of the study of quantum mechanical dynamics of strong-field generated ions is to directly observe and understand the ultrafast processes in the time domain. In order to accomplish this objective, a transient absorption experimental setup with a high spectral resolution has been installed at beamline FL26 after the FLASH II reaction microscope in FLASH DESY Hamburg. In this section, the experimental components of this study has been presented. This comprises of the FLASH which is the XUV-FEL light source, the fully synchronized HHG laser source available at the beamline[1] and an XUV transient -absorption setup. An overview of the setup is given in Fig 3.1.

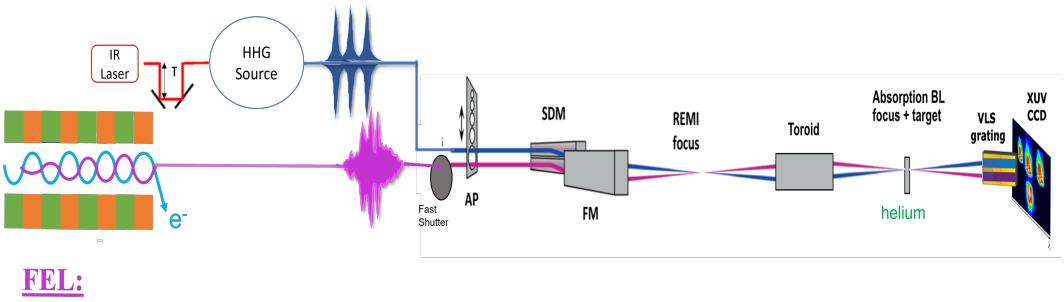

Figure 3.1: Schematics of the Experimental Setup[Figure adapted from [1]]

The last section will include the calibration done for the experimental setup and calculation for the temporal and spectral resolution of the setup.

3.1 Free Electron Laser(FEL) pulses from FLASH

FLASH, the Free-Electron LASer in Hamburg is the source of the intense, narrow bandwidth XUV and soft X-ray pulses. The laser is generated by accelerating the electrons using undulators in the synchrotron to produce radiation coherently. The FLASH facility consists of two distinct and mostly autonomous undulator lines, namely FLASH1 (Albert Einstein Hall) and FLASH2 (Kai Seigbahn Hall). The FLASH laser generation setup has been described in detail in Michael Straub's thesis[26]. This section will summarize the FEL

generation process and cover the basic principle of the FEL pulses necessary for understanding its purpose.

At FLASH, the pulse trains are generated by RF-gun based injector[21] then accelerated using undulators where the XUV radiation is generated. The undulators consists of an array of alternating magnetic poles, typically arranged in a periodic fashion that leads the electron bunches into a wiggle motion as in Fig3.1. The accelerated electrons undergo the spontaneous emission of photons. The central wavelength of this spectrally broad stochastic emission can be given by [14]:

$$\lambda_c = \lambda_u \frac{1 + K^2/2}{2\gamma^2} \tag{3.1}$$

where λ_u is the wavelength of a magnetic field oscillation generated by the undulators, and the dimensionless undulator strength $K = \frac{eB_0\lambda_u}{m_e c 2\pi}$, with the peak magnetic field B_0. The experiment was carried out at FLASH2 which has the ability to change the undulator gap manipulating the central wavelength from 3.3 to 90 nm in the fundamentals available in that facility.

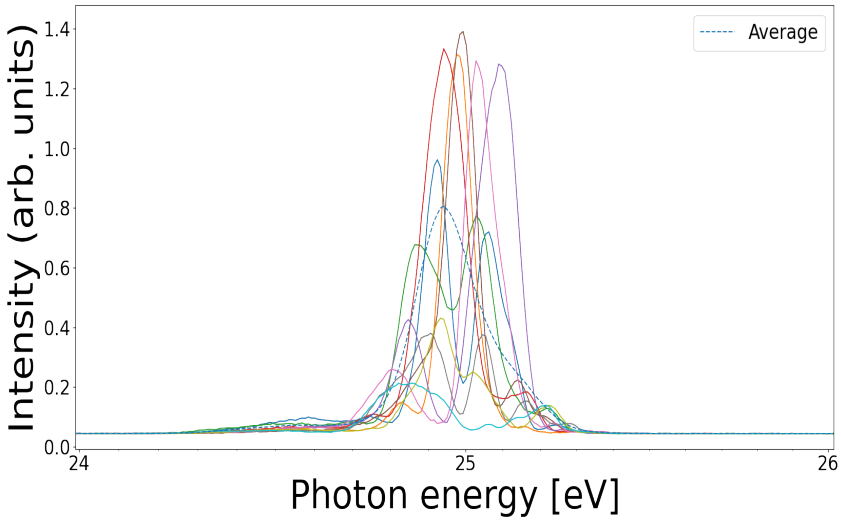

Figure 3.2: Stochastic Distribution of Free Electron Laser Pulses

The electrons interact with the photons generated by the initial spontaneous emission. This leads to a rapid and continuous increase in the emission of the photons until they reach a point of saturation or the undulator comes to an

end. This phenomenon is described as Self-Amplified Spontaneous Emission (SASE).

The pulses exhibit significant variations in terms of pulse structure and intensity on a shot-to-shot level as given in Fig 3.2. In this thesis, the FEL was tuned from 20 eV to 50 eV. The FEL pulse energy was set around 20 μJ with a repetition rate of 10 Hz in single bunches.

3.2 High Harmonic Generation(HHG) Source

The fully synchronized HHG laser source available at the beamline which offers ultrashort XUV pulses with wavelengths between 35 nm and 124 nm [1]. The higher harmonics produced for experimental purposes are displayed in Figure 3.3 in descending order of harmonic frequency.

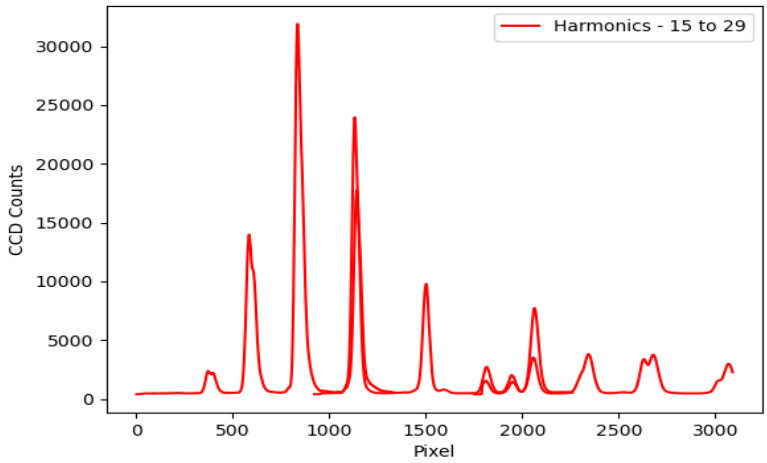

Figure 3.3: Harmonics observed at different camera position

In this section, the high harmonics generation from near-infrared (NIR) pulses has been described[23]. The rare gas medium of Krypton is enclosed within a gas cell that is similar absorption gas cell. The NIR pulses are focused into the gas cell to drive the high-order harmonic generation of the fundamental wavelength.

3.3 Transient Absorption Beamline

The HHG beam is integrated into the FEL beamline using an in-coupling mirror[1]. This mirror allows the HHG beam to enter the beamline parallel to FEL as shown in Fig 3.4.

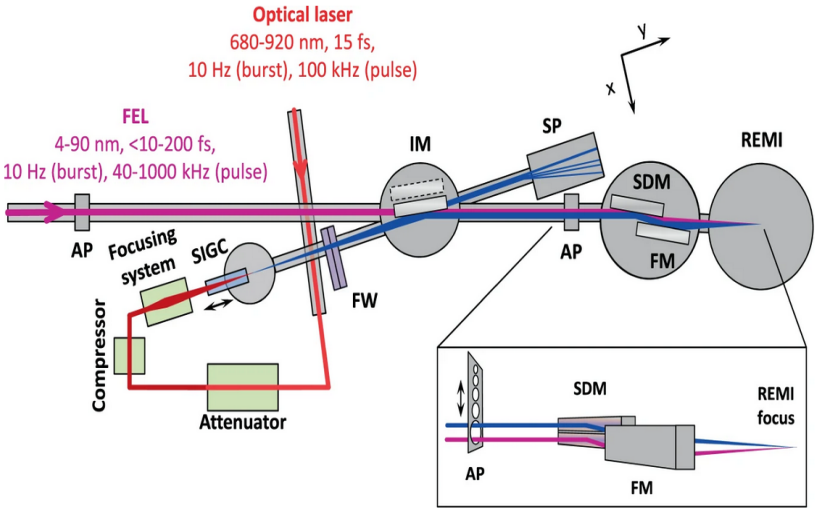

Figure 3.4: HHG source incorporated in the FEL beamline. SIGC: semi-infinite gas cell, FW: double filter wheel, IM: in-coupling mirror, AP: apertures array, SDM: split-and-delay mirror, FM: focusing ellipsoidal mirror, SP: spectrometer.[1]

The beams are focused into the Reaction Microscope (REMI), which is maintained in a state of ultra-high vacuum.

Downstream the REMI setup, the beams are refocused using a toroidal mirror [26] towards the gas absorption target as shown in Fig 3.5. The gas in the target gas cell is consistently kept at a specific backing pressure. The XUV FEL transmitted beam is obstructed as it is too intense for the spectrometer, nevertheless, a portion of the FEL light scatters and moves towards the grating. Next, the HHG beam and the FEL scattered light are placed onto a concave grating that is specifically designed for wavelengths ranging from 22 nm to 124 nm. The concave grating refocuses each specific wavelength onto the PIXIS camera, which possesses a range of around 11 eV.

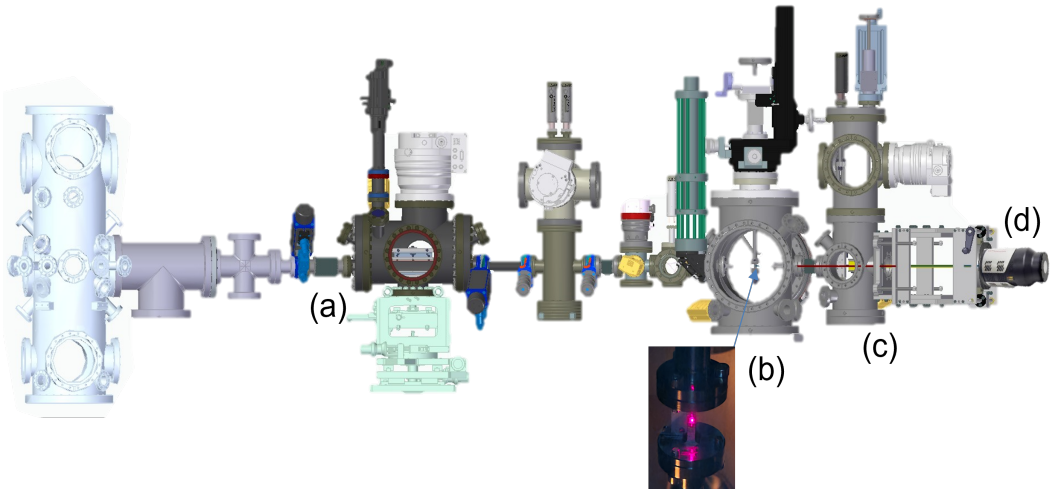

Figure 3.5: HHG FEL beamline: (a) Toroidal mirror (b) Target Gas cell (c) Grating chamber (d) PIXIS XUV Spectrometer

3.4 Photon Energy calibration

The PIXIS camera can be moved linearly to cover different energy ranges. In this section, the spectrometer has been energy-calibrated for a fixed camera position in the energy window between 20 and 30 eV. The spectrometer calibration was done using both Argon and Helium resonances. For argon, the $3s^2 3p^6\ ^1S \rightarrow 3s3p^6np\ ^1P$ resonances and for helium, the $1s^2\ ^1S \rightarrow 1snp\ ^1P$ resonances were observed at certain energies [9] as shown in Fig 3.6.

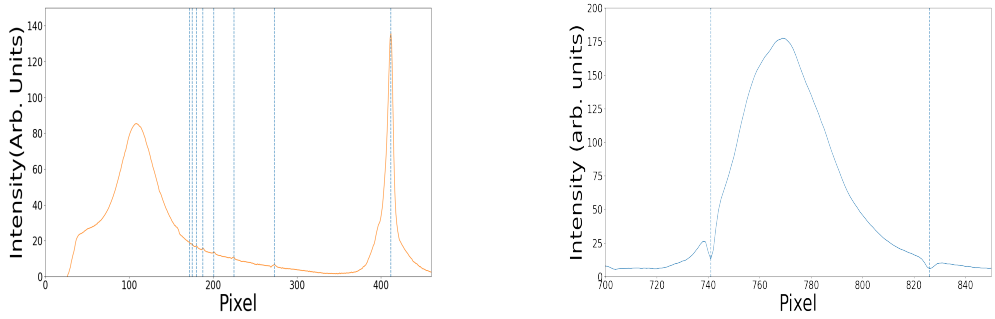

(a) Argon Resonances on transmitted spectra

(b) Helium Resonances on transmitted spectra

Figure 3.6: Argon Resonances with n=4,5,6,7,8,9,10,11 and helium resonances with n=3,4 are used for calibration (from right to left)

The argon resonances are autoionization resonances which involve the destructive interference of different pathways leading to the same continuum state such that the cross-section significantly drops on the resonance. As a consequence, there is an increase in transmission through the argon gas sample at the position of the resonances as shown in Fig 3.6a. The helium resonances are specific electronic transitions that are dipole-allowed from the ground state of the atom which leads to an increase in the cross-section of the resonance. As a consequence, there is a decrease in transmission through the helium gas sample at the position of the resonances as shown in Fig 3.6b.

The concave reflection grating in the spectrometer separates the various wavelengths of the spectrum. The schematics of the grating is given in Fig 3.7a. The dispersion of light of different wavelengths λ is given by

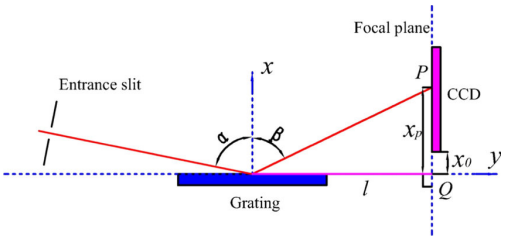

(a) Sketch of the Grating [Figure taken from [29]]

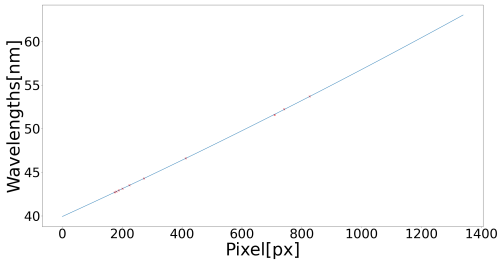

(b) Polynomial fit of the resonances

Figure 3.7: The spectrometer grating and its calibration

$$n\lambda = g[sin(\alpha) - sin(\beta)] \tag{3.2}$$

where n represents the spectral order of the dispersion, α is the incident angle and β is the reflected angle and g is the effective grating constant. The grating used in the spectrometer has a grating constant g = 1/600 mm for energies between about 20 eV to 112 eV [2]. Considering the schematics of the grating and spectrometer, the wavelength λ can be described as :

$$\lambda = \frac{g}{n}\left[sin(\alpha) - \frac{1}{\sqrt{\left(\frac{x_P}{l}\right)^2 + 1}}\right] \tag{3.3}$$

where x_P is the distance between the grating plane and where the light hits camera and l is the distance between grating and camera. The linear regression between the pixel position and the resonances given in Fig 3.7b is used to do the energy calibration.

3.5 Time Delay Calibration

The timings of both HHG and FEL have been recorded separately in Laser Arrival Monitor(LAM) and Beam Arrival Mointor(BAM) respectively. For initial estimation of temporal overlap an oscilloscope was used. In case of Argon, the disappearance of argon ion lines as shown in Fig 3.8 was used for the determination of temporal overlap.

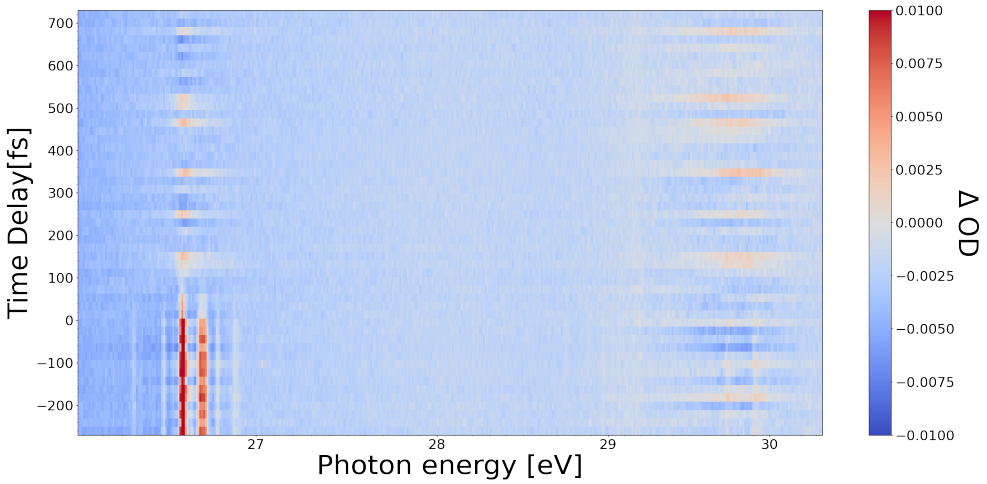

Figure 3.8: Argon Ion Yields

The pulses have relative temporal jitter and deviate in time from scan to scan, so for each scan it is necessary to determine the temporal overlap as shown in Fig 3.9. For initial determination of temporal overlap in the case of helium, the spectrally integrated lineouts have been fitted with eqn 3.4 to find out temporal overlap(t_0) as shown in Fig 3.10.

$$\Delta OD(t, E_r) = A_r(E_r)[1 - \Theta(t, t_0)(1 - e^{-\frac{t-t_0}{\tau}})] + B(E_r) \tag{3.4}$$

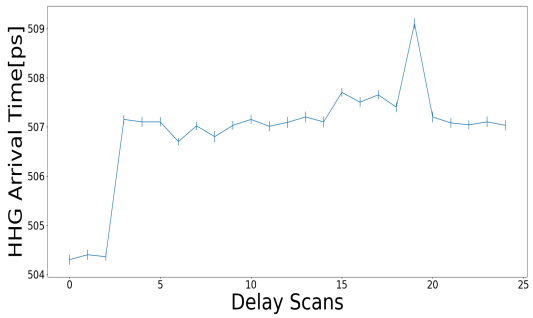

Figure 3.9: Temporal Overlap over Scans

It is observed in Fig 3.10 and Fig 4.11 that in case of FEL tuned above the first ionization threshold and only at certain gas pressure and FEL intensity, ionization of helium can produce a secondary peak is predicted as stark broadening feature as shown in Fig 3.11a [18].

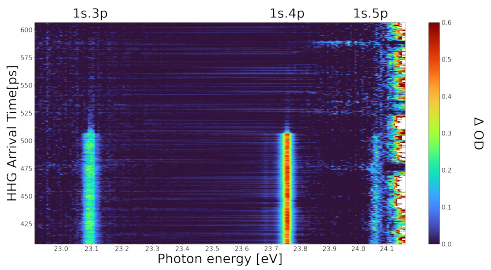

(a) Delay Scan Helium @ 30 mbar

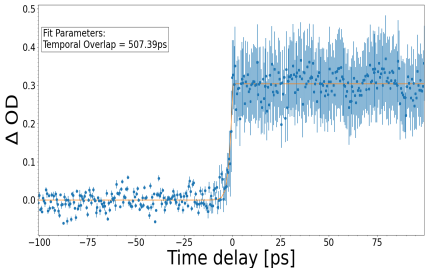

(b) Lineout of 1s4p Resonance

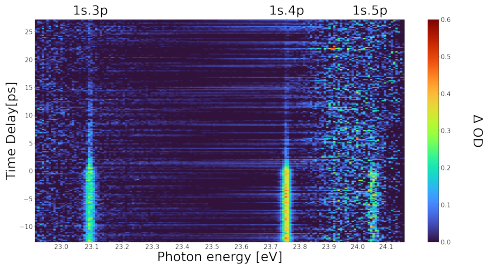

(c) Delay Scan Helium @ 16 mbar

Figure 3.10: Delay Scans — FEL tuned above 24.6 eV

So the most feasible way of determining temporal overlap and temporal jitter is fitting the lineouts with eqn 3.4. But for the ideal parameters, the secondary peak was observed at 23.68 eV near the 1s4s excited state at 23.673 eV as shown in Fig 3.11b which showed an instantaneous behaviour convoluted by temporal jitter. The lineout of the secondary peak was fitted with an error

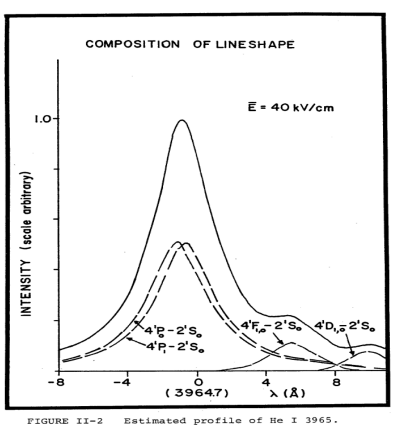

(a) Estimated profile of He I 3965[Figure Taken from [18]]

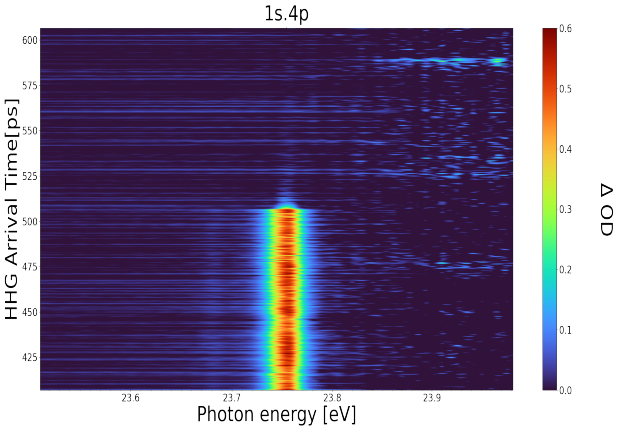

(b) 1s4s Sidefeature of 1s4p resonance from Fig 3.10a

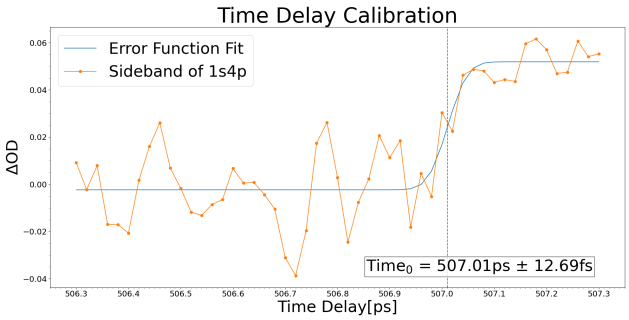

(c) Error fit on spectrally integrated Sidefeature

Figure 3.11: Time Delay calibration

function giving the precise temporal overlap as the centre of the slope of the error function and temporal resolution as the width of the error function slope which is around 110 fs which is observed in Fig 3.11c.

4 Transient Absorption spectroscopy

Transient Absorption Spectroscopy was done using the described setup. The time-delayed XUV HHG pulse and the intense XUV FEL are focused on the target cell after which they diverge. The XUV FEL transmitted beam is obstructed, nevertheless, a portion of the FEL light scatters and moves towards the grating. Subsequently, the transmitted radiation of the XUV HHG and the scattered FEL is quantified for each scan utilising the concave grating and the XUV PIXIS camera. The spectral time-delay scans were recorded automatically by programming in the different parameters such as the delay stage position for the pulse delay, the FEL intensity controlled by inserting Al filters of different thicknesses, different FEL photon energy and different delay parameters. The backing pressure of the target gas cell is changed manually using a gas delivery system. This chapter aims to highlight the procedure of data processing.

4.1 From transmission spectra to absorption spectra

The PIXIS camera with 1340×400 pixels captures the XUV transmitted light as an image and then produces a flat-field spectrum by integrating along the vertical axis. It was also noted that the FEL generates a substantial amount of broad background at lower energy levels. To account for this, background correction data was collected specifically for the FEL spectra corresponding to each dataset. Two sets of transmission spectrum are captured HHG+FEL and FEL only as shown in Fig 4.1a.

The reference spectrum could be acquired by measuring the transmission spectrum with and without helium in the target gas cell. However, the incident HHG intensity fluctuates from shot to shot, it would require a lot of data at a particular experimental setting to average out the fluctuations sufficiently. So, a fast shutter is employed to modulate the FEL beam, resulting in alternating spectra for the FEL pulse. Then the transmitted spectral intensity has been

recorded for each shot using an alternate FEL pulse in each spectra. The beam with HHG and helium serves as the reference, while the beams with HHG and FEL and helium are used to obtain the spectra. The HHG and FEL spectrum and FEL only spectrum are sorted for with and without FEL as shown in Fig 4.1b. The multiple scans of the transmitted spectrum of HHG and FEL and

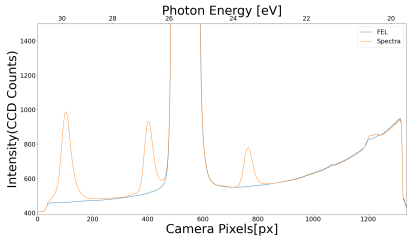

(a) Transmision Spectrum before sorting the spectra

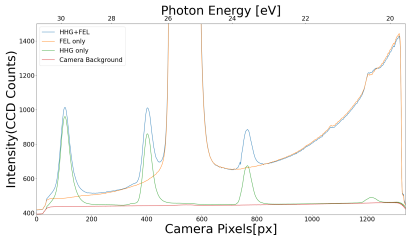

(b) Transmision Spectrum after sorting the spectra

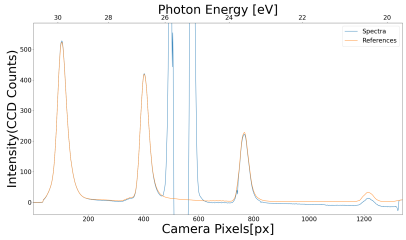

(c) Transmitted Spectrum after FEL Background Correction

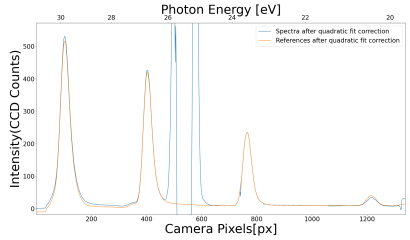

(d) Transmitted Spectrum after quadratic fit correction

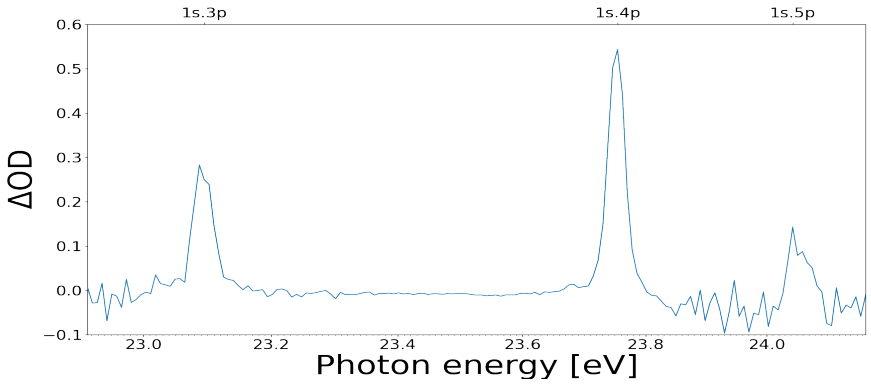

(e) Absorption Spectrum

Figure 4.1: Absorption Spectrum Data Processing

the reference spectrum of HHG are binned and averaged for each LAM value as given in Fig 4.1a. For greater statistics, the delay stage was moved back and forth as shown in Fig 4.2a. The transmitted spectrum of only the FEL

spectrum and the camera background is averaged.

The spectrum is energy calibrated using the calibration method described in

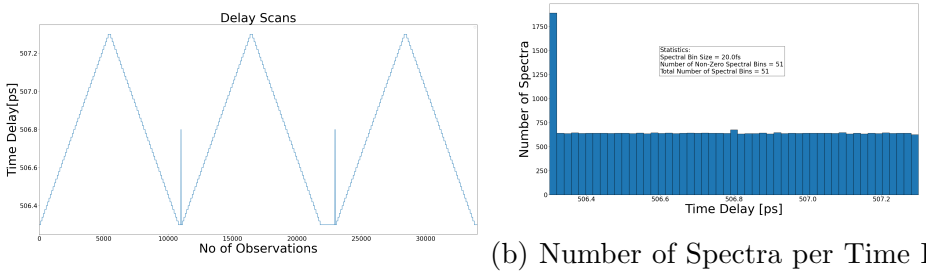

(a) Delay Scan Stage Movement

(b) Number of Spectra per Time Delay Value

Figure 4.2: Delay Stage Statistics

subsection 3.4. The FEL background correction was done by subtracting the FEL-only spectra from the HHG+FEL spectra as shown in Fig 4.1c. The resonant response was isolated by fitting with a quadratic function and subtracted as shown in Fig 4.1d. We calculate the absorption spectrum by calculating the relative optical density(ΔOD) using equation 4.1.

$$\Delta OD = -log_{10}\left(\frac{I(\omega)}{I_0(\omega)}\right) \tag{4.1}$$

The temporal overlap is determined using the process given in subsection

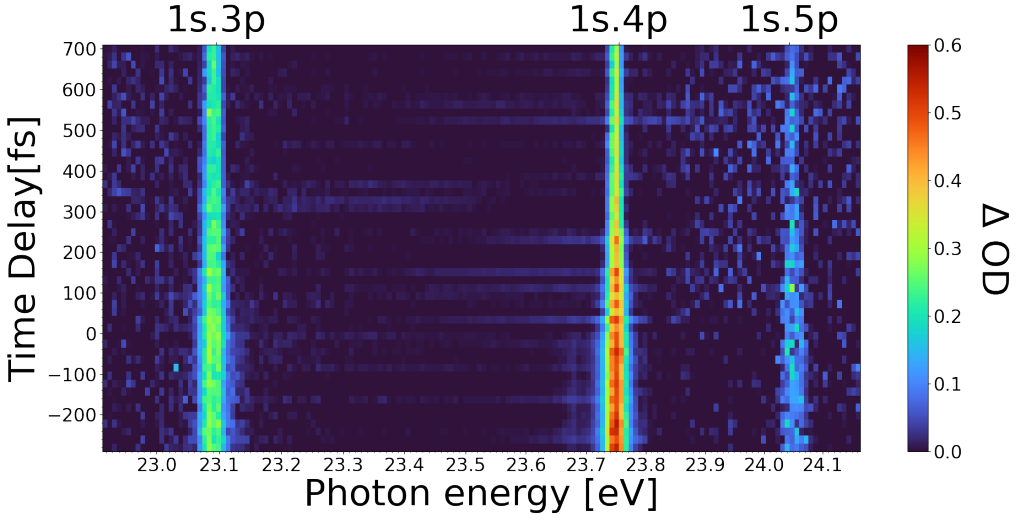

Figure 4.3: Absorption Spectra with each spectrum averaged over 650 scans

3.5. With the delay calibration, the delay-dependent scans are plotted with negative time delay in case of FEL precedes the HHG and the positive time delays for the case in which HHG precedes the FEL as given in Fig 4.3.

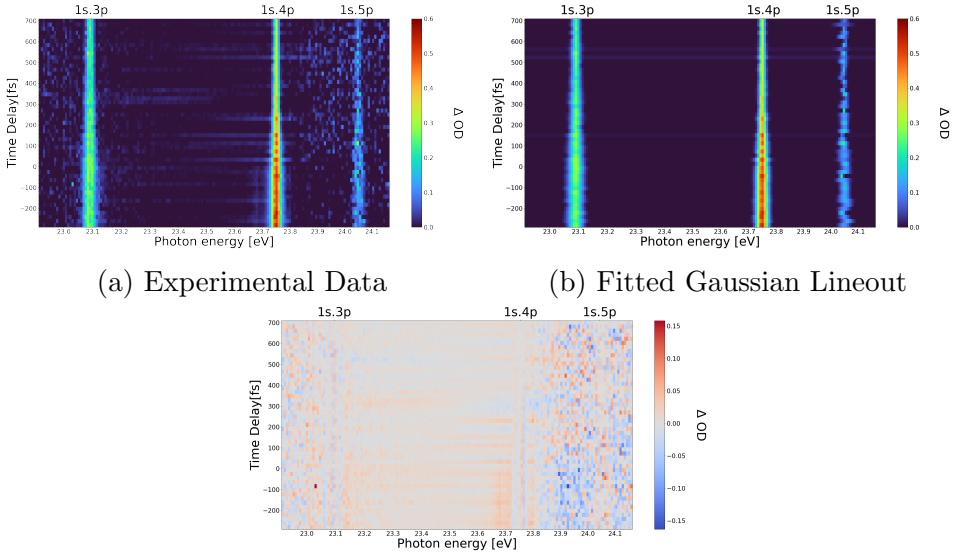

(a) Experimental Data (b) Fitted Gaussian Lineout

(c) Residue=Experiment-Fit

Figure 4.4: Lineout mapped using gaussian linshapes

The resonance peaks are theoretically Lorentzian in nature as given in subsection 2.3. But due to the spectrometer resolution of 15 meV, which is significantly larger than the natural absorption lineshape of the singly excited helium atoms, the lineshapes become Gaussian in nature after the convolution and the resonances can be mapped with Gausssian lineshapes as shown in Fig 4.4. It is verified by computing the residual as shown in Fig 4.4c.

4.2 State-resolved Dynamics

Analysing the resonance lineshape parameters allows for the extraction of the dynamics. The resonance parameters for 1s3p and 1s4p, including the on resonance amplitude, amplitude, and width obtained from the Gaussian fit, have been measured and quantified using the data from Figure 4.4. These parameters are then shown in Figure 4.5.

The dynamics of HHG first exhibit non-linear behaviour over time, charac-

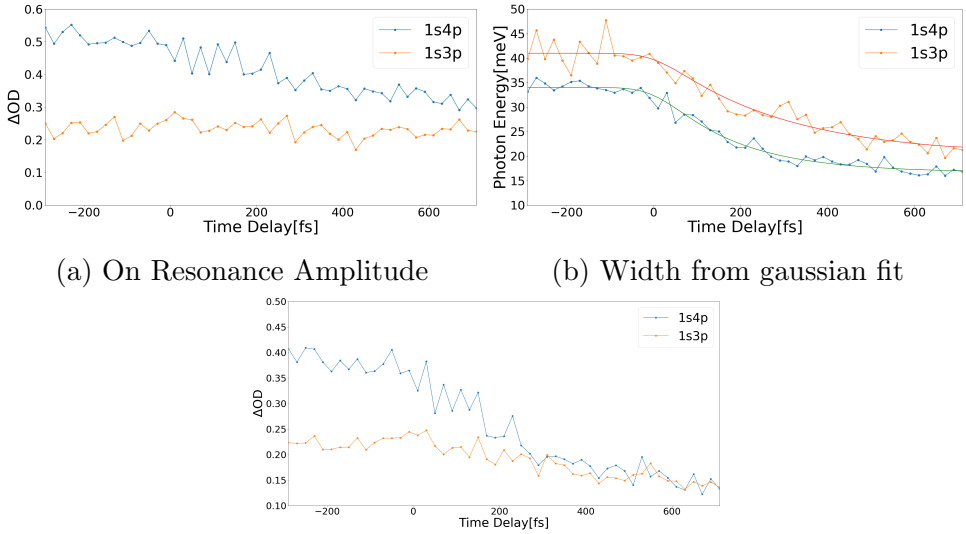

(a) On Resonance Amplitude (b) Width from gaussian fit

(c) Lineout averaged over 5 px

Figure 4.5: Lineout Resonance Parameters

terised by exponential decay. In contrast, the first case of free-electron laser (FEL) displays a continuous feature. The dynamics must consider the temporal variation between the two pulses, which is obtained in subsection 3.5. The dynamics could be written as given in equation 4.2:

$$\Delta OD(t, E_r) = e^{-\frac{t^2}{2\sigma^2}} * [A_r(E_r)\{1 - \Theta(t, t_0)(1 - e^{-\frac{t}{\tau_r}})\} + B(E_r)] \tag{4.2}$$

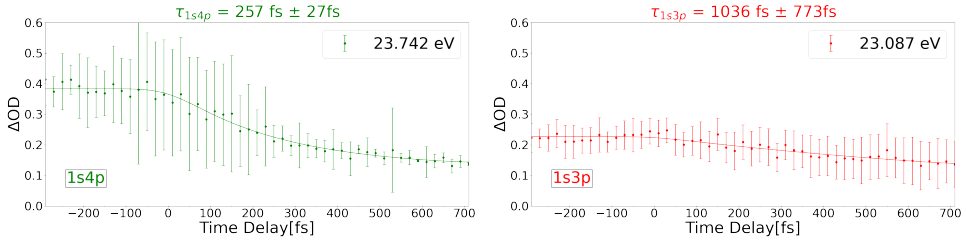

(a) 1s4p Resonance Dyanmics (b) 1s3p Resonance Dyanmics

Figure 4.6: Lineout fit

Here, E_r are the different resonant states, A_r is the maximum amplitude of the resonance peak over the time delay, τ_r is the exponential decay rate for each resonance state and B_r is the decay offset, t_0 is the temporal overlap between the two pulses.

The gaussian width of lineout of the resonances and the spectrally averaged lineout over 5 px around the resonances were fitted with eqn 4.2 as shown in Fig 4.5b and in Fig 4.6 and the fit parameters of the dynamics for 1s3p and 1s4p lineout width and spectrally averaged lineout has been tabulated in Table 4.1. The Table 4.1 demonstrates that Lineout exhibits a certain offset.

Table 4.1: Lineout fit values

State	1s4p	1s3p
Spectrally Integrated lineout		
Amplitude(A_r)	0.26	0.13
Decay Time(τ_r)	257fs	1036fs
Offset(B_r)	0.13	0.1
Width of Lineout		
Amplitude(A_r)	23.97 meV	40.99 meV
Decay Time($\tau_r 4$)	176.45fs	283.73fs
Offset(B_r)	0.00 meV	0.00 meV

However, with longer delay scans, as shown in Fig 4.7a, the resonance lines disappear. The accuracy of the fit is questionable.

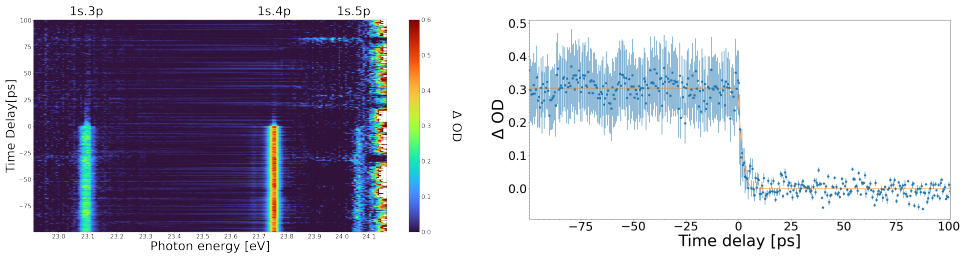

(a) Longer Delay Scans (b) Dynamics for longer scan

Figure 4.7: Lineout fit for Longer Delay Scans

In order to gain a more comprehensive understanding, larger delay scans were incorporated into the Lineout analysis, as depicted in Figure 4.7.

This was done to determine if the decay duration aligns with that of the shorter delay scans which has been tabulated in Table 4.2.

Table 4.2: Short and Long Delay Scan Fits

State	1s4p Short Scan	1s4p Long Scan
Spectrally Integrated lineout		
Amplitude(A_r)	0.26	0.3
Decay Time(τ_r)	257fs	1.4ps
Offset(B_r)	0.13	0.0

4.2.1 Stark induced 1s4s Transition

In the case of FEL first, due to the high intensity and pressure in the gas cell, a lot of the helium atoms get ionized and create plasma-like environment. The electric field due to the helium ions leads to the splitting of the 1s4p resonance state. The 1s4p split level overlaps with 1s4s state [20] which leads to stark induced distortion in the wavefunctions hence breaking the dipole selection rule and causing a collisional transfer equilibrium between these states[18].

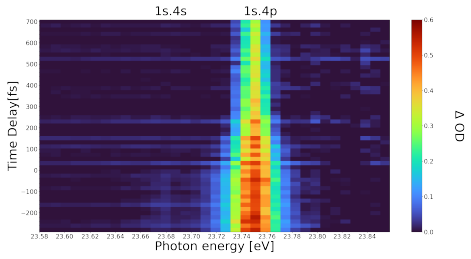

(a) 1s4s at 23.68 eV

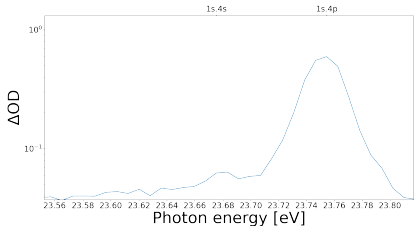

(b) 1s4s Lineshape

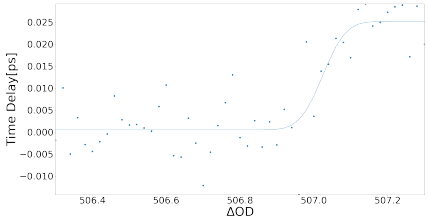

(c) 1s4s time delay evolution

Figure 4.8: 1s4s Sidefeature

This results in an asymmetric 1s4p lineshape with a small peak near 1s4s resonance 23.68 eV as shown in Fig 4.8b. The 1s4s peak shows an instantaneous

buildup from the time when FEL comes before HHG as shown in Fig 4.8c. This indicates towards the stark effect on 1s4p resonance state in case of FEL generated plasma in the gas cell.

Further in the chapter the 1s4p and 1s4s time delay dynamics have been extracted for different target cell backing pressure, different FEL intesity attenuated by different thickness of Aluminium filters and different FEL photon energy.

4.2.2 Pressure-dependent Scans

In order to observe the impact of pressure on the 1s4p resonance and 1s4s stark effect dynamics, the data was collected at various backing pressures of the target cell[1] as shown in Fig 4.9.

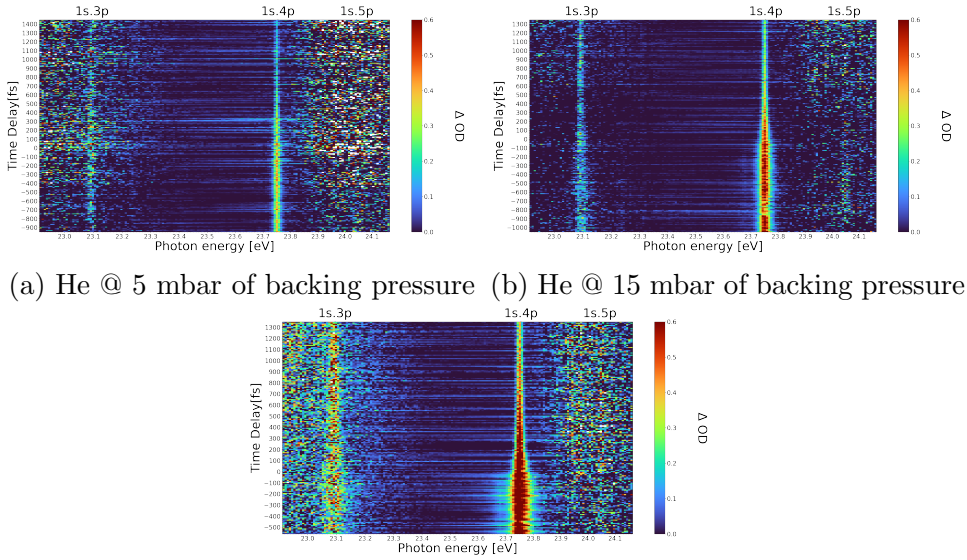

(a) He @ 5 mbar of backing pressure (b) He @ 15 mbar of backing pressure

(c) He @ 40 mbar of backing pressure

Figure 4.9: Pressure dependent Scans

The 1s4p resonance lineouts were taken for different backing pressures as shown in Fig 4.10a. The stark induced 1s4s transition lineouts were also taken for

[1]Backing Pressure of the target gas cell is not the pressure in the Gas Cell as it works in a gradient within the pipes

different pressures as shown in Fig 4.10b.

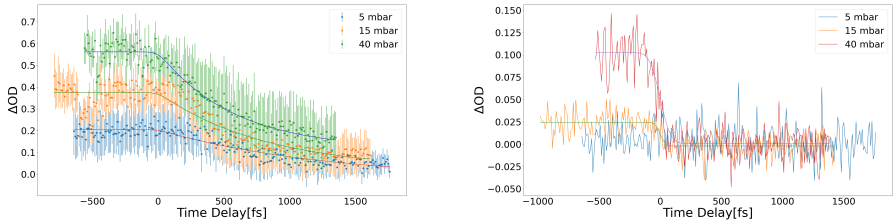

(a) 1s4p Dynamics (b) 1s4s Dynamics

Figure 4.10: Resonance Dynamics for different target cell backing pressure

The dynamics of 1s4p resonance is fitted with eqn 4.2 and the dynamics parameters were tabulated for comparison in Tab. 4.3. An evident correlation can be noted between the increase in pressure and the significant increase of maximum absorption, as well as the reduction in decay lifetime. It can also be noticed that the 1s4s transition is almost non-existent in case of low pressure due to low stark effect from the lesser number of charged particles.

Table 4.3: Pressure Dependent Dynamics of 1s4p Resonance

Pressure	5mbar	15mbar	40mbar
Lineout of 1s4p resonance			
Amplitude(A_r)	0.22	0.35	0.44
Decay Time(τ_r)	1263	808	572
Offset(B_r)	0	0	0.11

It states that as the number of atoms in the gas cell increases, the number of collisions also increases, resulting in a shorter collision time. This leads to temporal and energy uncertainty in the transition process. As a result, the lineshape broadens. Additionally, the number of charged particles increases leading to increase in the electric field due to charged particles, which perturbs the energy levels of the electron. Consequently, the interaction of the excited

atom with the electric field leads to a shift in the energy levels, leading to a broadening of the lineshape. The resonance crossection increases with pressure but is narrow in nature hence gets saturated on the transmitted spectrum and gets convoluted by the spectrometer resolution leading to a broadened lineshape which will be explained in detail in section 5.

4.2.3 Intensity dependent Scans

In order to determine the dependence of resonance dynamics on FEL intensity, the FEL has been attenuated by inserting Aluminium(Al) filters of few nm thickness[2]. The spectrum data collected for different attenuation of FEL with the constant central FEL photon energy as shown in Fig. 4.11.

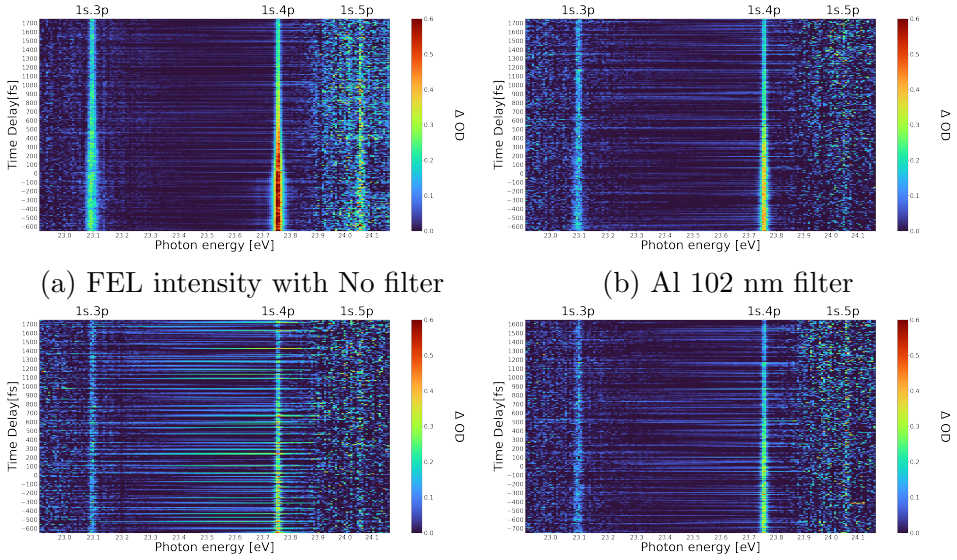

(a) FEL intensity with No filter

(b) Al 102 nm filter

(c) Al 204 nm filter

(d) Al 204 nm filter

Figure 4.11: Intensity dependent Scans

The spectrally integrated and offresonant background corrected lineouts of the 1s4p resonance are recorded for different Al filter setting as shown in Fig. 4.12.

The dynamics of 1s4p resonance is fitted with eqn 4.2 and the dynamics pa-

[2]The FEL intensity may be inversely proportional to thickness of the filter if filter material has a high absorption coefficient in the energy range of the FEL

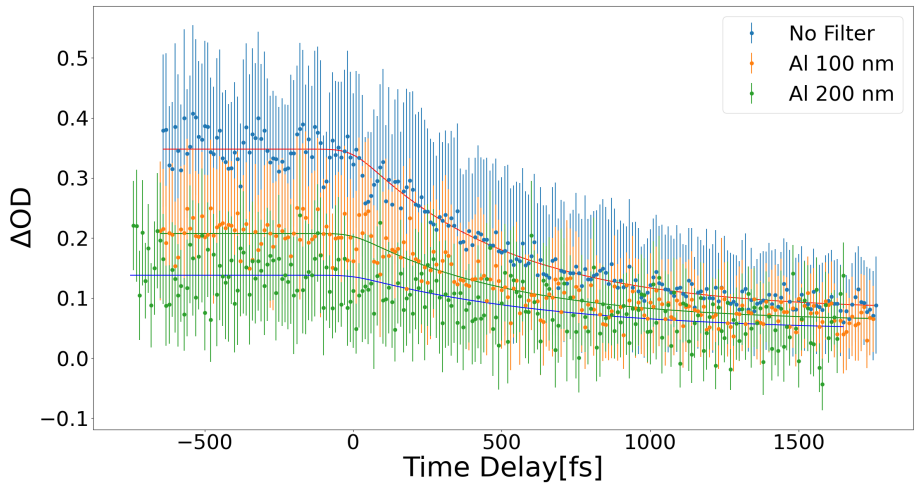

Figure 4.12: Intensity Resonance Dynamics

rameters were tabulated for comparison in Tab. 4.4. It is evident from the graph that the maximum absorption increases and the decay lifetime decreases with the decrease in the thickness of Al filter and hence increase in the FEL intensity.

Table 4.4: Intensity Dependent Dynamics of 1s4p Resonance

Thickness of Aluminum Filter	No Filter	100 nm	200nm
Lineout of 1s4p resonance			
Amplitude(A_r)	0.27	0.15	0.09
Decay Time(τ_r)	508 fs	526.5 fs	665 fs
Offset(B_r)	0	0	0

The reduced intensity of the FEL results in a lower flux of photons, which in turn leads to a decreased ability to ionise helium atoms. Consequently, there is a less quantity of charged particles, resulting in a diminished Stark effect caused by the electric field generated by these charged particles. The decay lifetime increases when the stark effect weakens, resulting in less disruption in the energy levels and a less power broadening effect. This implies that the FEL dressed state is comparatively closer to the natural state. The 1s4s state

is observed only when there are no filters and there is a substantial plasma density resulting from the presence of charged particles.

4.2.4 FEL Photon Energy dependent Scans

The effect of FEL photon energy on the resonances has been studied by tuning FEL photon energy between 20 eV and 40 eV. These scans were taken with fixed delay setting of positive delay(HHG first), temporal overlap and negative delay(FEL first) as shown in Fig 4.13.

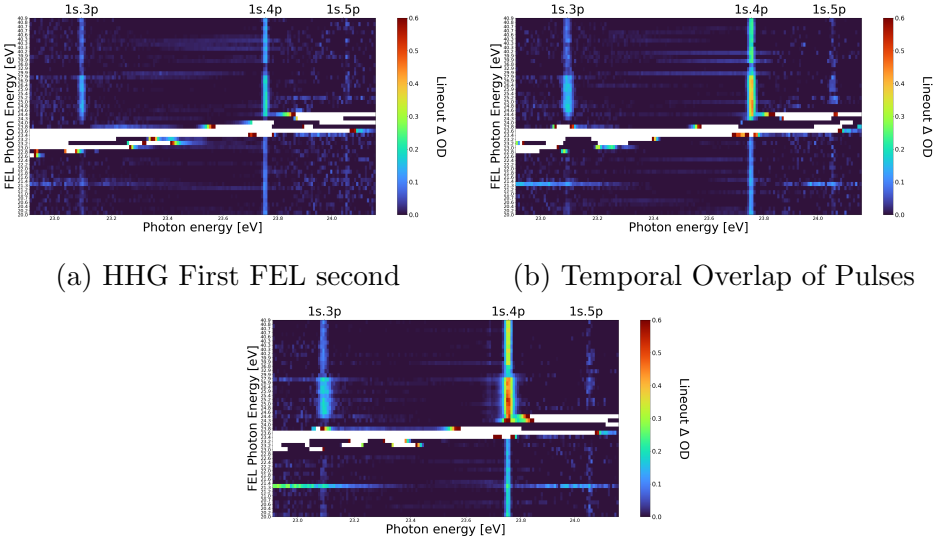

(a) HHG First FEL second

(b) Temporal Overlap of Pulses

(c) FEL first HHG second

Figure 4.13: FEL Photon Energy dependent Scan

It can be observed that when FEL photon energy is tuned below the first ionization threshold, in the case of FEL first, the FEL excites a lot of helium atoms to singly excited states. Then due to interaction between two excited helium atoms, two excited atoms can undergo collision-induced ionization, this generates few ions increasing the absorption by a little bit in FEL first regime. [3]

Three different interaction mechanism were studied by tuning the photon energy of FEL and look into resonant and non-resonant XUV-driven nonlinear

[3] Absorption Spectrum cannot be calculated in case of spectral overlap of HHG and FEL

dynamics. In the first case, the FEL was tuned between 20 eV and the first ionization threshold i.e., 24.6 eV to align the FEL singly excited state resonances such 1s2p at 21.2 eV, 1s3p at 23.08 eV, 1s4p at 23.74 eV. In this case, the intense FEL pulse was assumed to resonantly couple $1s^2$ and 1snp atomic levels within the coherence time of HHG excited dipole and will lead to strong Rabi oscillations but as seen in Fig 4.14a no such signature was recorded.

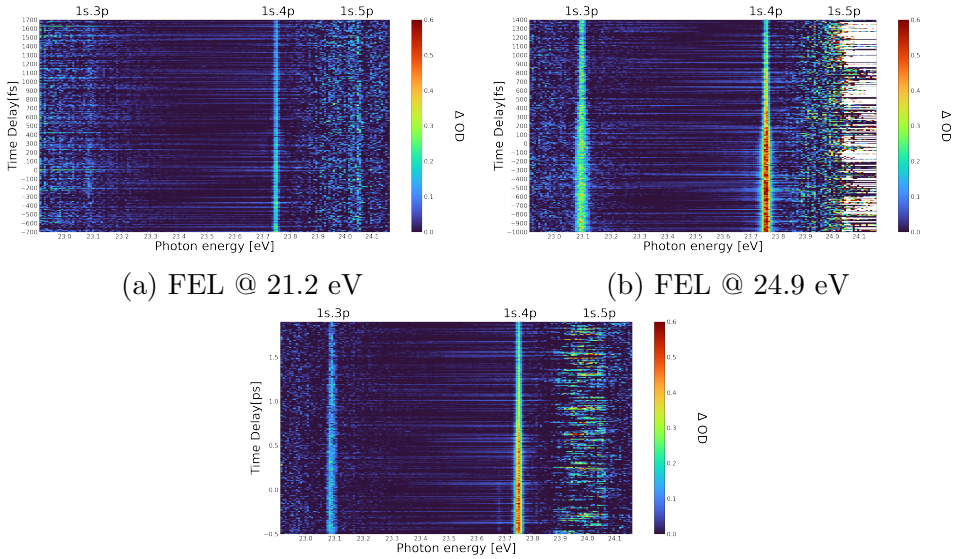

(a) FEL @ 21.2 eV

(b) FEL @ 24.9 eV

(c) FEL @ 40 eV

Figure 4.14: Photon Energy dependent Scans

In the second case, the FEL was tuned above the single-ionization threshold of helium at 24.6 eV in order to ionize the ground state and cause the plasma effect as shown in Fig 4.14b. This case shows an ultrafast exponential decay of the resonance lineshape in the case of HHG first or the positive time delay region.

In the third case, the FEL was tuned to about 40 eV so that the second electron of 1s4p excited helium can be excited to 2p4p state at 64 eV as shown in Fig 4.14c. It was anticipated to observe a steplike structures as wiggles on the the 1s4p resonance.

5 Dipole Response for FEL induced Plasma Environment

The dipole control model has been developed in [3], [4] and [24] to provide the framework for understanding the time-delay-dependent, spectroscopic datasets. This model describes the physical interpretations of the experimental results given in chapter 4 and helps in understanding the correlation between the time and the frequency domain in a comprehensive manner. This model has been adapted for a prolonged effect of perturbed environment interaction and it incorporates the effect of spectrometer resolution and the saturation of very narrow lineshapes of singly excited states of helium.

5.1 Dipole Evolution in ionized environment:

The atoms in an excited state are not isolated and are not stationary. The inherent spectral lineshape of resonance in individual atoms is very narrow. Consequently, they will encounter collisional broadening and Doppler broadening in the spectrum domain as discussed in subsection 2.5. These processes decrease the lifetime of the dipole response. The temporal dipole response function $f_1(t)$ for the gas-induced decay of oscillating dipole moment was derived in subsection 2.3.

$$d(t) = id_{0j}^2 e^{i\omega_r t - \frac{\Gamma}{2}t} = f_1(t) \tag{5.1}$$

The dipole control model as described in earlier works deals with the impulsive interaction of the δ-like dressing laser field with the dipole response. However, in the case of an ionized environment due to the intense XUV laser, the interaction of dipole-excited atoms with the ions happens throughout the dipole evolution. It is hypothesised that the ionised environment behaves similarly to an error function, and its continuous interaction results in continuous per-

turbation. As a result, there is a smooth transition from a gradual decay of the dipole response induced by gas to a faster decay throughout the evolution of the dipole response. This can be described as the neutral environment response being modified with a faster Gaussian decay.

$$G(t,\tau) = e^{-(t-\tau)^2/2\sigma^2}$$

It is important to note that when $t < 0$ i.e., when the excitation pulse has not been transmitted yet, the atoms remain unexcited and the excited state is vacant, resulting in no dipole response.
This event may be categorised into two scenarios based on whether the intense FEL pulse arrives before or after the initiation of dipole response. :

First Case: In this scenario, the FEL tuned above the ionization threshold is first transmitted, causing the ionisation of a significant number of neutral helium atoms. This results in the creation of an environment that remains ionised and relatively stable during the dipole response period. After a time delay τ at t=0, the XUV HHG pulse arrives and stimulates the dipole response in the few remaining neutral helium atoms in the ionised medium. This response has a rapid decrease from the beginning, which is not influenced by the time delay. In the spectral domain from the Fourier transform of the temporal dipole response, a constant broad peak is observed due to the constant short lifetime of the dipole response[4].

$$d_\tau(t,\tau) = \begin{cases} 0 & \text{if } t < 0 \\ G(t,0) f_1(t) & \text{if } t > 0 \end{cases} \tag{5.2}$$

Second Case: In this scenario, the XUV excitation pulse is initially applied at t=0, stimulating the dipole response. The dipole response then undergoes

[4]When the oscillating function is defined over a short period in the temporal domain, there is more uncertainty in its frequency. As a result, in the spectral domain, we see a wide peak.

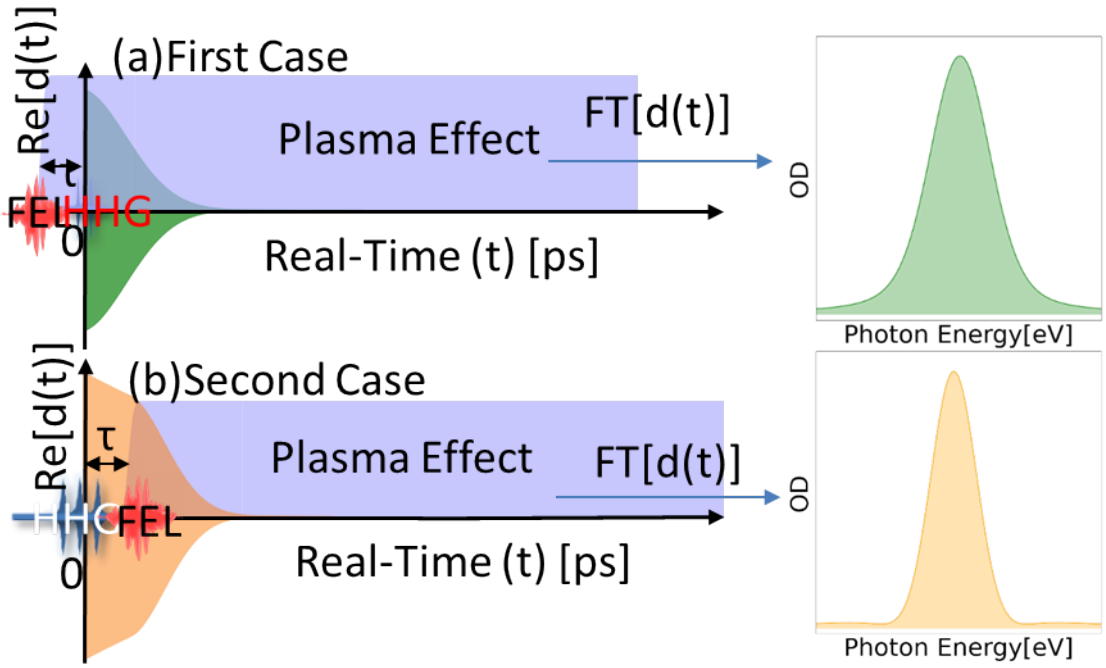

Figure 5.1: Dipole Control Model for sustained interaction:(a)When FEL comes before HHG and ionizes the gas cell and creates an ionized environment and the neutral helium atoms are excited in the ionized environment (b)When HHG comes before FEL and excites the dipole response which decays naturally and then after some time delay τ, the FEL comes and perturbs the dipole response

decay due to the presence of gas until the XUV FEL, which is tuned above the ionisation threshold, arrives and ionises neutral helium atoms. However, the excited helium atoms are not affected by this ionisation. Instead, the ionised environment interacts with the dipole response, leading to a faster decay characterised by a Gaussian shape. This dipole response depends on the delay between the two pulses. In the spectral domain, as the delay increases, the temporal dipole response is characterised by an extended duration, resulting in less uncertainty in its frequency and a narrower peak.

$$d_\tau(t,\tau) = \begin{cases} 0 & \text{if } t < 0 \\ f_1(t) & \text{if } 0 < t < \tau \\ G(t,\tau) f_1(t) & \text{if } t > \tau \end{cases} \tag{5.3}$$

5.2 From time-domain to Spectral Domain

When studying spectroscopy, the spectral domain representation of the dipole response is obtained instead of the time-domain representation. The computation of the absorption spectrum involves Fourier transforming the array of dipole response values in the spectral domain[5].

$$\tilde{d}(\omega) = FT[d(t)] \tag{5.4}$$

The spectral distribution of the absorption cross-section is directly proportional to the imaginary component of the Fourier transform of the dipole response, as stated in equation from [28]

$$\sigma(\omega) = 4\pi g \alpha \omega Im \left[\frac{FT[d(t)]}{E(\omega)} \right] \tag{5.5}$$

5.3 Effect of Spectrometer Resolution

When comparing the theoretical photoabsorption crosssection to the experimental optical density, it is important to take into account the limitations of the spectrometer. One such limitation is the finite spectrometer resolution, which becomes particularly relevant when dealing with narrow spectral widths and high crosssections, such as those observed in singly excited resonances in helium.

In order to consider the spectrometer's resolution, it is necessary to convolve the transmitted spectrum, rather than the absorption spectrum, with the spectrometer's resolution function i.e., a normalized gaussian function K(ω) given by [2]:

$$K(\omega) = \frac{1}{\sqrt{2\pi}\sigma_r} e^{\frac{-\omega^2}{2\sigma_r^2}} \tag{5.6}$$

[5] Analytical Fourier transformation of the dipole response if not possible due to complexity of the dipole response function

The incident spectrum, namely the XUV HHG pulses, is modelled using a Gaussian spectral profile. The profile has a centre energy, b, of 23.55 eV, a peak intensity of 1 unit, and a Gaussian RMS width, c, of 7 units.

$$I_0 = ae^{-\frac{(x-b)^2}{2c^2}} \tag{5.7}$$

The transmitted spectrum is determined using the Beer-Lambert exponential attenuation law.

$$I = I_0 e^{-\rho l \sigma(\omega,\tau)} \tag{5.8}$$

where l is the length of the gas cell and ρ is the density of the gas.

$$\rho = \frac{M}{RT} P \tag{5.9}$$

where P is the pressure in mbar, M is the molar mass of helium and T is the room temperature.

By convolving the spectrometer resolution function with the transmission

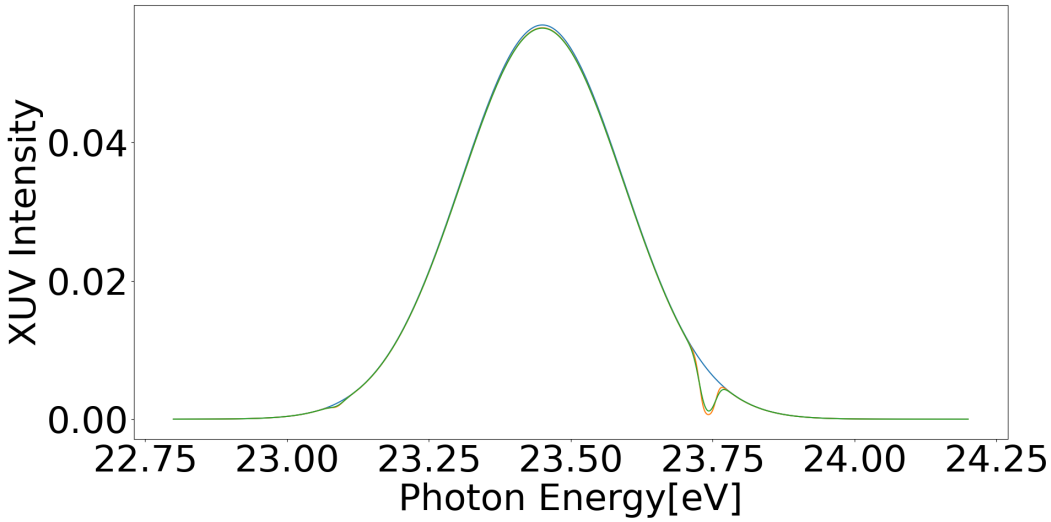

Figure 5.2: Transmitted Spectrum after convolution

spectrum, we get the absorbance that is shown.

$$A\text{“}(\omega) = -log_{10}\left(\frac{K(\omega) * I}{I_0}\right) \tag{5.10}$$

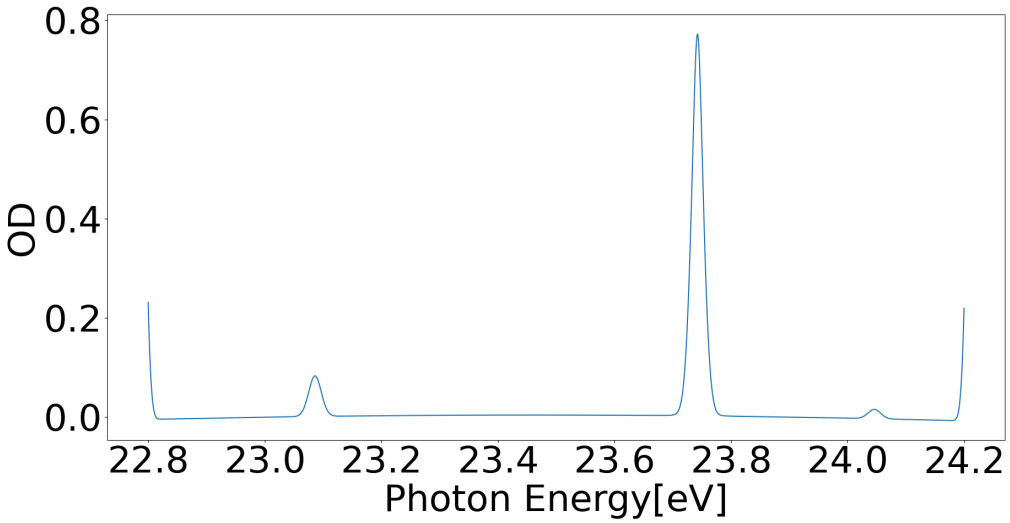

Figure 5.3: Absorption Spectrum calculated using Beer Lambert's Law

This method effectively suppresses the absorbance of the resonant transitions. In summary, the low resonant absorption lines detected in the test, despite their large cross-section, may be attributed to the convolution of the transmission spectrum with the limited resolution of the spectrometer.

5.4 Comparison with Experimental Results

An absorption spectrum array is calculated by computing the absorption spectrum for a range of delays, resulting in a delay-dependent absorption spectrum array. For the purpose of comparison with experimental data we take 1s4p resonance as our focus and take the on-resonance amplitude in both cases. To get a preliminary understanding, the spectrometer resolution was tuned to the resolution of the spectrometer from the experiment i.e., 15 meV and the parameters including d_0j, $gamma$ and gas pressure were individually changed while keeping the others constant. The on-resonance amplitude was then extracted from the absorption spectrum array and shown in Fig5.4

The model was manually adjusted to align with the experimental data based on these tendencies.

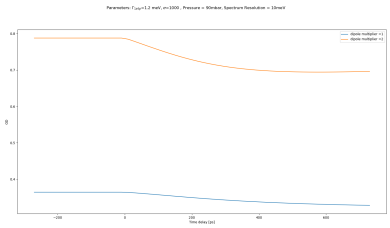

(a) For different dipole matrix element d_{ge}

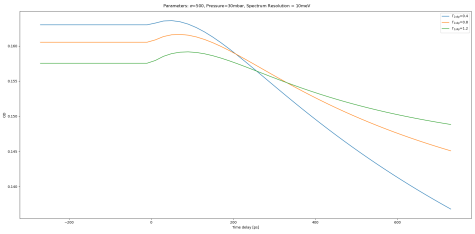

(b) For different decay width γ

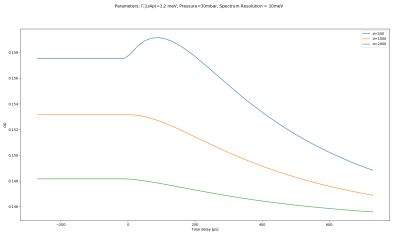

(c) For different dipole control parameter

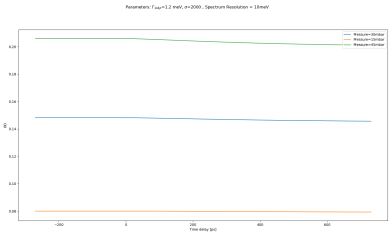

(d) For different pressure

Figure 5.4: On-resonance amplitude trends for different paramters

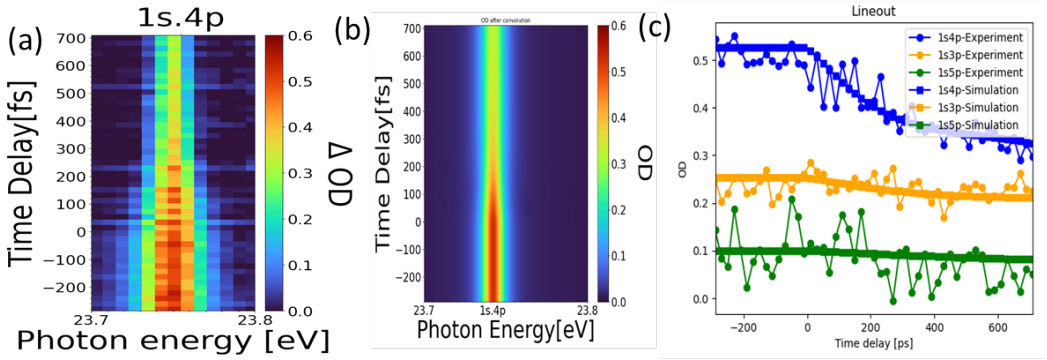

Figure 5.5: Comparison between the measured optical density of resonance 1s4p and the simulated optical density

6 Summary and Conclusions

The main theme of this thesis focuses on the time-resolved study of ionization triggered by intense femtosecond extreme ultraviolet(XUV) free-electron laser(FEL) pulses. Although there has been significant research on the interaction between intense XUV light and matter, as well as the behaviour of extreme ionisation [27][5], the real-time dynamics of a quantum system in the context of XUV light-matter interaction have not been studied by reconstructing XUV-modified dipole responses, as has been done for NIR-modified dipole responses[24]. FEL control HHG probe mechanism was used in XUV transient absorption spectroscopy to monitor the XUV light-matter interaction in a time-resolved manner similar to the XUV pump- XUV probe dynamics [8][16]. The XUV HHG is used to excite the electrons in a coherent manner, resulting in the generation of an XUV-induced dipole response. The response interferes with the XUV HHG pulses, and the interference is measured using transient absorption spectroscopy. The dipole response is further modified by the XUV FEL pulse and its impact has been measured over time by capturing the XUV transient absorption spectra at various time delays between the XUV HHG and XUV FEL.

The measurements were taken at beamline FL26 FLASHII, DESY during a beamtime in August 2023. The beamline has been equipped with an XUV spilt-delay mirror which has a temporal resolution of 50 fs and an XUV spectrometer which has a spectral resolution of 14.6 meV. The XUV HHG peaks were discreet and in the range of 20-30 eV and the single XUV FEL peak had a bandwidth of 0.3 eV and was tuned between 20 and 40 eV with the goal to resonate with the singly excited states, to directly ionize the helium atoms and to add the possibility to excite the second electron of the HHG excited atoms to the doubly excited states. The spectrometer was calibrated using argon lines as a reference. Two sets of measurements were conducted for each configuration: one with both HHG and FEL, and another with just FEL.

These scans were performed using a laser chopper operating at a frequency of 10 Hz, which blocked every second FEL pulse. The two sets of measurements are sorted to identify the presence of FEL. This results in four different data sets: HHG and FEL, which represents the main spectrum data; HHG only, which serves as the reference spectrum; FEL only, which is used to correct for the background generated by intense FEL and normalise the main spectrum data; and the camera background, which is used to normalise the HHG reference. The absence of an in-situ reference without any gas necessitated the use of this data to compute the change in optical density rather than the optical density, resulting in the observation of the change in lineshape structure.
The high intensity of a FEL ionizes a huge population of helium atoms which causes significant distortion in the electron cloud, effectively allowing transitions that are otherwise forbidden by dipole selection rules. Because the appearance of this forbidden transition is dependent upon the prior manifestation of FEL, the termination of the forbidden transition may be used to determine temporal overlap between FEL and HHG pulses. The initial studies focused on identifying the optimal conditions for the backing pressure of the gas cell and the attenuation of FEL. These conditions were chosen to ensure that forbidden transitions could be clearly distinguished from the background noise. If the FEL arrives early, the dipole response is affected by the ionised environment. This effect diminishes within a millisecond, which is consistent with the timeframe of the dipole response. Consequently, the absorption spectrum remains unchanged under these circumstances. Therefore, the dynamics of the delay-dependent absorption spectra were also used to ascertain the temporal overlap between the XUV HHG and XUV FEL. In the case of FEL first, the spectrally integrated lineouts and the width of the 1s4p resonance remain constant. However, in the case of HHG first, they exponentially decrease on a picosecond period and eventually disappear.

The dipole control model was developed for impulsive light-matter interaction[3].

However, this thesis aims to modify the model in order to include a sustained interaction between the ionised environment created by the FEL and the excited helium atoms. The excited atoms are not in a state of isolation and are not stationary. The natural spectral lineshape of single-atom resonance is quite narrow. As a result, they will experience collisional broadening and Doppler broadening in the spectrum domain. These phenomena reduce the lifetime of the dipole response. The interaction can be categorised into two cases: 1. If the ionised medium is formed prior to resonant excitation, it results in a perturbed decay of the temporal dipole response, resembling a half Gaussian distribution. This leads to a broad Gaussian resonance peak in the spectral domain. 2. If the ionised medium is formed after a certain time delay following resonant excitation, it causes a gas-induced decay of the dipole response. However, once the ionised medium is rapidly built up by the arrival of FEL, it again undergoes a perturbed decay resembling a half-Gaussian distribution. This results in a narrower peak compared to the first case. The spectral lineshape remains narrower than the resolution of the spectrometer, even after accounting for these broadenings. As a result, the transmitted spectrum is convoluted with a Gaussian spectrometer function[2]. Subsequently, the absorption spectrum is computed for various time delay values. The delay-resolved absorption spectra was analysed to determine the resonant lineouts. The impact of several factors, including spectrometer resolution, temperature, pressure, and dipole transition matrix components, on the width and amplitude of the resonance lineshape was investigated. An effort was made to compare the model's findings with the experimental data.

It is further aimed to look into the calculation of the number density and temperature of plasma-like ionized environment and how it evolves the time.

A Appendix

A.1 Dipole Matrix Elements of Helium

Table A.1: The dipole matrix elements between the 1sns and 1snp series of the singly excited bound states of helium. The dipole matrix elements are given in atomic units.

	$1s^2$	1s2s	1s3s	1s4s
1s2p	0.729	5.057	1.870	0.656
1s3p	0.36	1.580	12.382	4.628
1s4p	0.227	0.801	2.671	22.714
1s5p	0.160	0.515	1.352	4.003
1s6p	0.121	0.371	0.874	2.001

A.2 Argon Transition Lines

Table A.2: The Energies of $3s3p^6np$ singly excited states of Argon were taken from [9]

State	Energy(eV)
$3s^23p^6$	0
$3s3p^64p$	26.617
$3s3p^65p$	27.99
$3s3p^66p$	28.51
$3s3p^67p$	28.75
$3s3p^68p$	28.89

References

[1] Elisa Appi, Christina C Papadopoulou, Hannes Lindenblatt, Florian Trost, Severin Meister, Patrizia Schoch, Rolf Treusch, Robert Moshammer, Ingmar Hartl, Uwe Morgner, and Milutin Kovacev. A synchronized VUV light source based on high-order harmonic generation at FLASH. *Sci. Rep.*, 10(1):6867, April 2020.

[2] Paul Birk. *The Dipole Response of an Ionization Threshold within Ultrashort and Strong Fields*. Phd thesis, Ruperto-Carola-University of Heidelberg, 2020.

[3] Alexander Blättermann. *Impulsive control of the atomic dipole response in the time and frequency domain*. Phd thesis, Ruperto-Carola-University of Heidelberg, 2016.

[4] Alexander Blättermann, C. Ott, A. Kaldun, T. Ding, and T. Pfeifer. Two-dimensional spectral interpretation of time-dependent absorption near laser-coupled resonances. *J. Phys. B: At. Mol. Opt. Phys.*, 2014.

[5] C Bostedt, M Adolph, E Eremina, M Hoener, D Rupp, S Schorb, H Thomas, A R B de Castro, and T Möller. Clusters in intense FLASH pulses: ultrafast ionization dynamics and electron emission studied with spectroscopic and scattering techniques. *J. Phys. B At. Mol. Opt. Phys.*, 43(19):194011, October 2010.

[6] R. W. Boyd and Nonlinear Optics. *3rd ed.* (Elsevier LTD, Oxford, 2008.

[7] Wolfgang Demtröder. *Atoms, Molecules and Photons An Introduction to Atomic-, Molecular- and Quantum Physics*. Springer, 2010.

[8] Thomas Ding, Marc Rebholz, Lennart Aufleger, Maximilian Hartmann, Veit Stooß, Alexander Magunia, Paul Birk, Gergana Dimitrova Borisova, Christian Ott, and Thomas Pfeifer. XUV pump-XUV probe transient

absorption spectroscopy at FELs. *Faraday Discuss.*, 228(0):519–536, May 2021.

[9] NIST: Atomic Spectra Database Energy Levels Form.

[10] M. A. Gigosos, S. Djurovi´c, I. Savi´c, D. González-Herrero, Z. Mijatovi´c, and R. Kobilarov. Stark broadening of lines from transition between states n =3 to n = 2 in neutral helium. *AA 561, A135*, 561, Oct 2013.

[11] M. A. Gigosos, S. Djurovi´c, I. Savi´c, D. González-Herrero, Z. Mijatovi´c, and R. Kobilarov. Stark broadening of lines from transition between states n =3 to n = 2 in neutral helium. *AA 561, A135*, 561, Oct 2013.

[12] Gigosos, M. A., Djurović, S., Savić, I., González-Herrero, D., Mijatović, Z., and Kobilarov, R. Stark broadening of lines from transition between states n=3 to n=2 in neutral helium - An experimental and computer-simulation study . *AA*, 561:A135, 2014.

[13] P. Hamm and M. Zanni. *Concepts and Methods of 2D Infrared Spectroscopy*. Cambridge University Press, Cambridge, 2011.

[14] K.-J. Kim, Z. Huang, and R. Lindberg. *Synchrotron Radiation and Free-Electron Lasers: Principles of Coherent X-Ray Generation*. Cambridge: Cambridge University Press, 2017.

[15] T. Kita, T. Harada, N. Nakano, and H. Kuroda. Mechanically ruled aberration-corrected concave gratings for a flat-field grazing-incidence spectrograph. *Applied Optics*, 22:512–513, February 1983.

[16] Alexander Magunia, Marc Rebholz, Elisa Appi, Christian Ott, and Thomas Pfeifer. Time-resolving state-specific molecular dissociation with XUV broadband absorption spectroscopy. *Sci. Adv.*, 9(47):eadk1482, November 2023.

[17] Aurelia Alonso Medina. Measurement of laser-lnduced plasma: Stark broadening parameters of pb(ii) 2203.5 and 4386.5 a spectral lines. *Phys. Rev. Lett.*, 121, Oct 2018.

[18] Peter James Pilon. Stark broadened he i 3965 (4p-2s), 1978.

[19] E. Sadeghzadeh Lari, H. Ranjbar Askari, M. T. Meftah, and M. Shariat. Calculation of electron density and temperature of plasmas by using new Stark broadening formula of helium lines. *Physics of Plasmas*, 26(2):023519, 02 2019.

[20] Jayanta K Saha, T K Mukherjee, P K Mukherjee, and B Fricke. Effect of strongly coupled plasma on the magnetic dipolar and quadrupolar transitions of two-electron ions. *Phys. Plasmas*, 20(4):042703, April 2013.

[21] S. Schreiber. The injector of the vuv-fel at desy. volume p. THPP038, 2005.

[22] S. Schreiber and B. Faatz. The free-electron laser FLASH. *High Power Laser Science and Engineering*, 3, 2015.

[23] Veit Stooβ. *Strong-Field Spectroscopy: From Absorption to Time-Resolved Dynamics in Strong Fields.* PhD thesis, Ruperto-Carola-University of Heidelberg, Germany, 2018.

[24] V. Stooß, S. M. Cavaletto, S. Donsa, A. Blättermann, P. Birk, C. H. Keitel, I. Březinová, J. Burgdörfer, C. Ott, and T. Pfeifer. Real-Time Reconstruction of the Strong-Field-Driven Dipole Response. *Phys. Rev. Lett.*, 121, Oct 2018.

[25] V. Stooß, S. M. Cavaletto, S. Donsa, A. Blättermann, P. Birk, C. H. Keitel, I. Březinová, J. Burgdörfer, C. Ott, and T. Pfeifer. Real-Time Reconstruction of the Strong-Field-Driven Dipole Response. *Phys. Rev. Lett.*, 121:173005, Oct 2018.

[26] Michael Straub. Multiphoton ionization of helium with extreme ultraviolet light at the free-electron laser in hamburg. Master thesis, University of Heidelberg, 2021.

[27] H Wabnitz, L Bittner, A R B de Castro, R Döhrmann, P Gürtler, T Laarmann, W Laasch, J Schulz, A Swiderski, K von Haeften, T Möller, B Faatz, A Fateev, J Feldhaus, C Gerth, U Hahn, E Saldin, E Schneidmiller, K Sytchev, K Tiedtke, R Treusch, and M Yurkov. Multiple ionization of atom clusters by intense soft x-rays from a free-electron laser. *Nature*, 420(6915):482–485, December 2002.

[28] Mengxi Wu, Shaohao Chen, Seth Camp, Kenneth J Schafer, and Mette B Gaarde. Theory of strong-field attosecond transient absorption, volume=49, doi=10.1088/0953-4075/49/6/062003. *Journal of Physics B: Atomic, Molecular and Optical Physics*, (6):062003, Feb 2016.

[29] Gang Xiong, Jiyan Zhang, Guohong Yang, Jiamin Yang, Hang Li, Zhimin Hu, Yang Zhao, Minxi Wei, and Tao Yi. Different approaches to precise wavelength calibration of a flat-field grating spectrometer for laser-produced plasmas. *Phys. Scr.*, 89(6):065005, June 2014.